EUROPEAN ORGANIZATION FOR NUCLEAR RESEARCH

CERN–SPSC–2010–022
SPSC-M-772
September 3, 2010

# COMPASS-II Proposal: Questions & Answers

*The COMPASS Collaboration*

contact: A. Magnon/CEA-Saclay, G. K. Mallot/CERN
COMPASS spokespersons
Alain.Magnon@cern.ch, Gerhard.Mallot@cern.ch

**Introduction**
This document presents the answers to the questions on the COMPASS-II Proposal SPSC-P-340 posed by the Referees following the SPSC meeting on 29–30 June, 2010. Each question from Q 1 to Q 23 is repeated in italics and followed by an answer in roman starting with "A:".

**Notation**
In the text the following notation is used in the answers sections: References in italics, *e.g. Fig., Eq., p.*, refer to the original proposal, while references in roman, *e.g.* Fig., Eq., p., refer to the present document.

# ChPT measurements

**Q 1:** *Chiral perturbation: we would like to be convinced that you will clearly advance the significance of the data relative to what exists.*

A: What exists in terms of experimental values for the pion polarisability has been summarised in the proposal very briefly as "different experimental approaches, affected by large uncertainties and discrepancies". In Table 1 we give a more detailed list of these attempts. They are grouped by the three processes which have been proposed in order to access the desired pion–photon scattering: Pion Primakoff scattering, radiative pion photoproduction and photon–photon collisions. The wide spread of the experimental data is illustrated in Fig. 1.

Table 1: Experimental values of $\alpha_\pi, \beta_\pi,\ (\alpha_\pi + \beta_\pi),\ (\alpha_\pi - \beta_\pi)$

| Data | Reaction | Parameter | Value $[10^{-4}\ \mathrm{fm}^3]$ |
|---|---|---|---|
| Serpukhov ($\alpha_\pi + \beta_\pi = 0$)[1] | $\pi Z \to \pi Z \gamma$ | $\alpha_\pi$ | $6.8 \pm 1.4 \pm 1.2$ |
| Serpukhov ($\alpha_\pi + \beta_\pi \neq 0$)[2] | | $\alpha_\pi + \beta_\pi$ | $1.4 \pm 3.1 \pm 2.8$ |
| | | $\beta_\pi$ | $-7.1 \pm 2.8 \pm 1.8$ |
| Lebedev [3] | $\gamma N \to \gamma N \pi$ | $\alpha_\pi$ | $20 \pm 12$ |
| Mami A2 [4] | $\gamma p \to \gamma \pi^+ n$ | $\alpha_\pi - \beta_\pi$ | $11.6 \pm 1.5 \pm 3.0 \pm 0.5$ |
| PLUTO [5] | $\gamma\gamma \to \pi^+\pi^-$ | $\alpha_\pi$ | $19.1 \pm 4.8 \pm 5.7$ |
| DM1 [6] | $\gamma\gamma \to \pi^+\pi^-$ | $\alpha_\pi$ | $17.2 \pm 4.6$ |
| DM2 [7] | $\gamma\gamma \to \pi^+\pi^-$ | $\alpha_\pi$ | $26.3 \pm 7.4$ |
| Mark II [8] | $\gamma\gamma \to \pi^+\pi^-$ | $\alpha_\pi$ | $2.2 \pm 1.6$ |
| Global fit: MARK II, VENUS, ALEPH, TPC/2$\gamma$, CELLO, BELLE (L. Fil'kov, V. Kashevarov)[9] | $\gamma\gamma \to \pi^+\pi^-$ | $\alpha_\pi - \beta_\pi$ | $13.0^{+2.6}_{-1.9}$ |
| | | $\alpha_\pi + \beta_\pi$ | $0.18^{+0.11}_{-0.02}$ |
| Global fit: MARK II, Crystal Ball (A. Kaloshin, V. Serebryakov) [10] | $\gamma\gamma \to \pi^+\pi^-$ | $\alpha_\pi - \beta_\pi$ | $5.25 \pm 0.95$ |

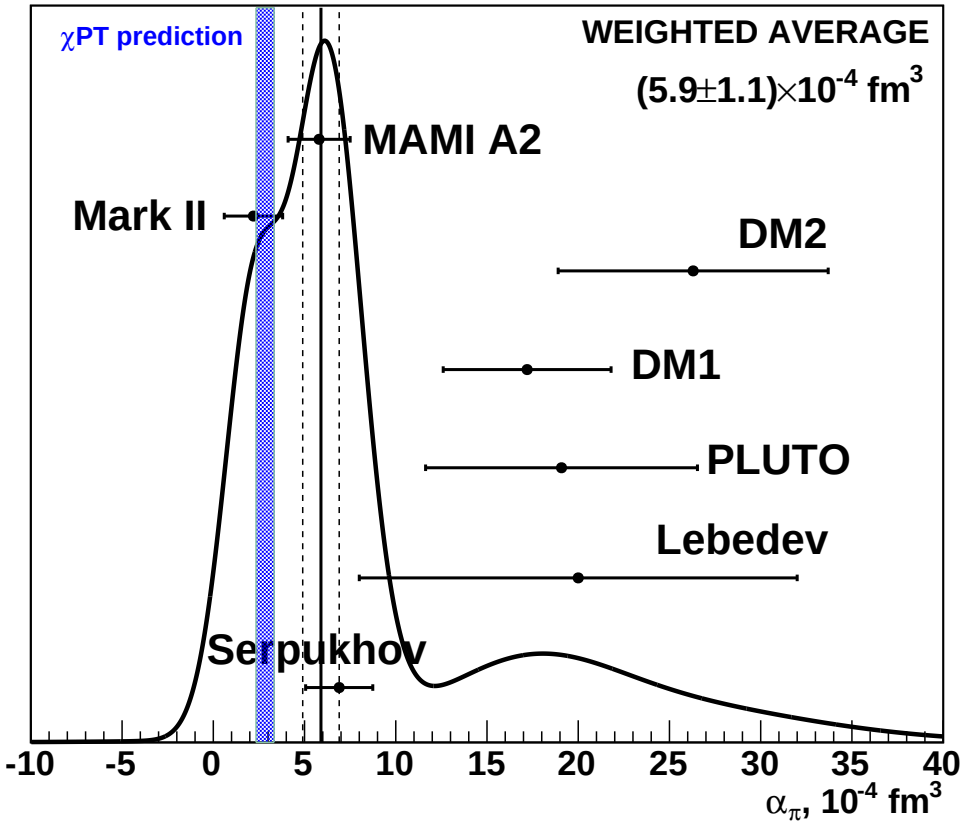


Figure 1: Global fit to the experimental data on the pion polarisability $\alpha_\pi$ as given in Table 1. The curve represents an ideogram of the data and their errors as described and used in the Review of Particle Physics [11] (cf. Sect. 5.2.2 therein).

As a general critique of the $\gamma\gamma \to \pi\pi$ experiments, we cite M.R. Pennington [12]:

> "[...] All this means that the only way to measure the pion polarisabilities is in the Compton scattering process near threshold and not in $\gamma\gamma \to \pi\pi$. Though the low energy $\gamma\gamma \to \pi\pi$ scattering is seemingly close to the Compton threshold [...] and so the *extrapolation* not very far, the dominance of the pion pole [...] means that the energy scale for this continuation is $m_\pi$. Thus the polarisabilities cannot be determined accurately from $\gamma\gamma$ experiments in a model-independent way and must be measured in the Compton scattering region."

In this spirit the $\gamma\gamma \to \pi\pi$ data are to be understood rather as a supplement to Compton scattering data than an independent way to determine the polarisabilities: Due to the indirect relation (via $s \leftrightarrow t$ crossing) with $\pi\gamma$ scattering, the important threshold region (where the polarisabilities are defined) remains inaccessible, and the $\gamma\gamma$ data are rather sensitive to the loop contributions than to the polarisabilities. Consequently, the attempts to determine polarisabilities from $\gamma\gamma$ reactions alone are affected by a wide spread of extracted polarisability values, as they strongly depend on the theoretical assumptions that must be made in the analysis.

Embedding the real Compton scattering process in radiative pion production, on the other hand, is accompanied by the systematic uncertainty due to the baryonic contributions in the considered diagrams [4], which has been criticised to be only insufficiently accounted for by the so-called "model-dependence error" estimation [4, 13].

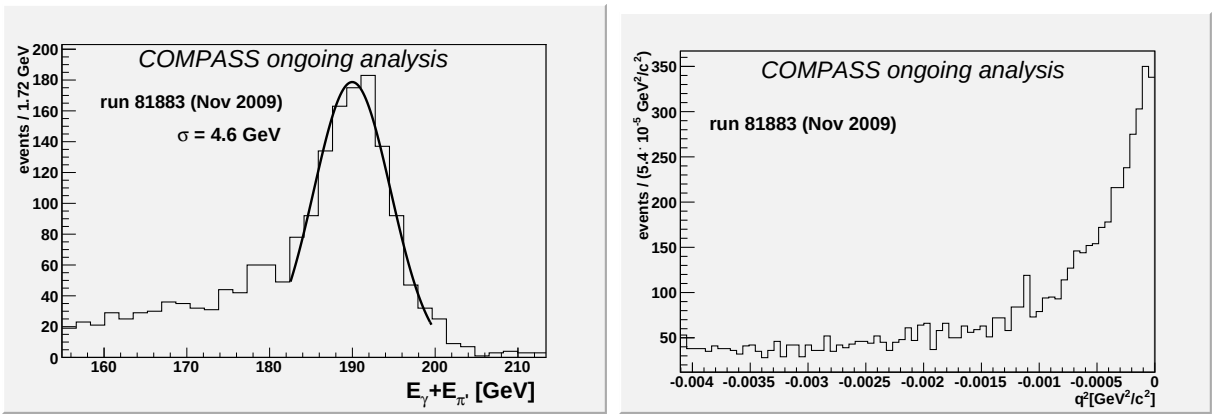


Figure 2: Left: Events with exclusive $\pi\gamma$ final state in 2009 data (run 81883, about 1/40 of expected statistics). Right: Identification of the electromagnetic contribution through the Primakoff peak in $q^2$ near zero.

So the task to determine the pion polarisabilities with a small and controllable systematic uncertainty remains to be accomplished with Primakoff scattering, for which the COMPASS experiment is a unique facility to reach a new level of precision compared to the earlier Serpukhov experiment. The data taken in an about 2-week period in 2009 (for details see answer to Q2) are expected to deliver a new value for $\alpha_\pi$, analogously to Ref. [1], with a smaller statistical error. A determination of $\alpha_\pi$ and $\beta_\pi$ as two independent parameters will only be possible with a large uncertainty, albeit again smaller than that of Ref. [2]. It is the opportunity of the proposed new measurement to experimentally establish a possible deviation of $\alpha_\pi + \beta_\pi$ from zero as predicted by ChPT. This prediction would be $5\sigma$ from zero given the expected experimental precision. Furthermore, tagging of the kaon component in the beam will allow for the determination of the kaon polarisability for the first time.

**Q 2:** *p 76: can you show results of the 2009 data taking?*

A: From a first analysis of one run taken in 2009, we show the exclusivity peak in the $\pi\gamma$ final-state energy and the Primakoff signal in Fig. 2. As a consequence of the changes in the calorimeter and target setup with respect to 2004, we find a higher resolution by at least 20% in both distributions.
This enhancement is not a final value yet, since here only a preliminary cell-wise calibration has been applied, extracted from the data themselves. For the final calibration, a dedicated subgroup of six Ph.D. students and postdocs has formed, with the goal to use the full information of the LED and neutral pion signals for a decent run-by-run calibration. While about 3/4 of the work is estimated to be done, a few more months will have to be invested into this task.
One challenge in this endeavour is the new trigger hardware that came in the experiment as add-on in the last weeks of the 2009 data taking. This new hardware allows for a very good time resolution ($\sim$ 1 ns) and for a signal shape analysis (32 samples) and, most importantly, the new digital trigger, which worked smoothly after commissioning.

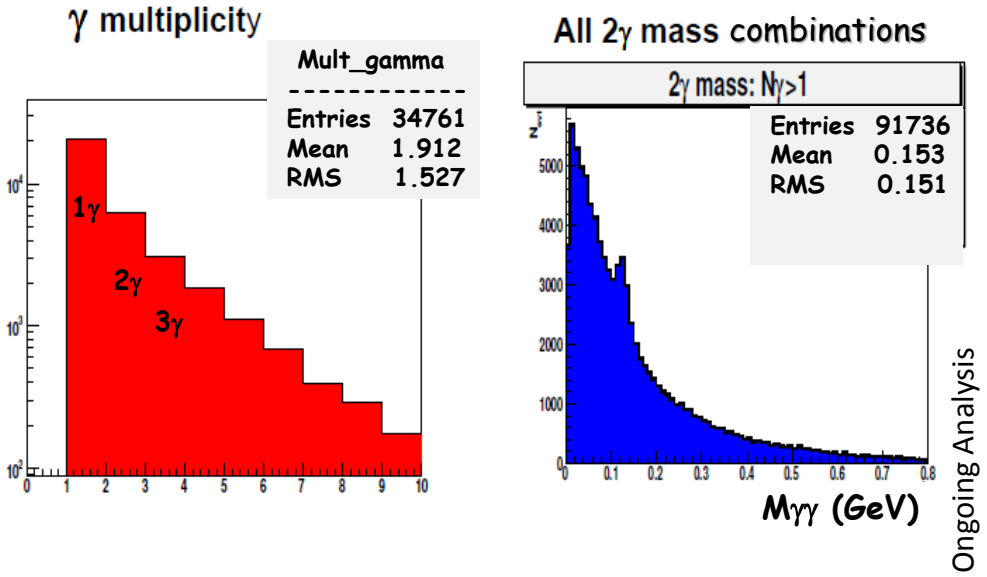


Figure 3: Photon multiplicity and possible $2\gamma$ mass combinations for the preselected sample: one recoil proton, at least one $\gamma$ of energy larger than 5 GeV (10 GeV) in ECAL1 (ECAL2). The ECALs timing cuts have been applied.

# DVCS and GPDs

**Q 3:** *We would like to see more details on the method to estimate possible pi0 background to DVCS and to see what it gives in 2009 data.*

A: A background to Deeply Virtual Compton Scattering (DVCS) arises from exclusive production of $\pi^0$s where one of the two $\gamma$'s from $\pi^0$ decay is not detected by the electromagnetic calorimeters and therefore may fake a DVCS event.
We had a first look at exclusive $\pi^0$ production using the 2008 DVCS test data, however statistics was not sufficient to conclude. Significant information on the production of $\pi^0$s is derived from a first analysis of the 2009 data [14]. The preselected sample is identical to the one for DVCS [15] and the ECAL timing information is used as was done in the final 2008 data analysis [16]. Figure 3 shows for this sample the photon multiplicity and the mass spectrum of the $2\gamma$ combinations. In the forthcoming analysis only those $2\gamma$ events ($\sim 20\%$) are considered for which at least one $\gamma$ had an energy larger than 5 GeV (10 GeV) in ECAL1 (ECAL2).
Since most of the DVCS events are located in ECAL1 [17] we consider from now on only the events where the $2\gamma$'s are detected in ECAL1 with at least one $\gamma$ of energy larger than 5 GeV.
In a first step, we try to estimate background contributions to DVCS from events containing a $\pi^0$. Figure 4 (top) shows the $2\gamma$ mass spectrum keeping only the $Q^2 > 1$ $(\mathrm{GeV}/c)^2$ events. The $\pi^0$ mass peak is prominent. As will be discussed below, a cut requiring $\cos(\theta) < 0.8$ ($\theta$ is the photon angle in the centre-of-mass system of the decaying $\pi^0$) has been applied which cleans up the $\pi^0$ signature. In total, 184 events are found in the $\pi^0$ mass peak.
In order to estimate the possible background to DVCS we have assumed that only the high-energy photon $\gamma_1$ from a $\pi^0$ decay is detected and the event is analysed as a valid DVCS candidate. Figure 4 (bottom) shows the energy distribution of the parent $\pi^0$ for

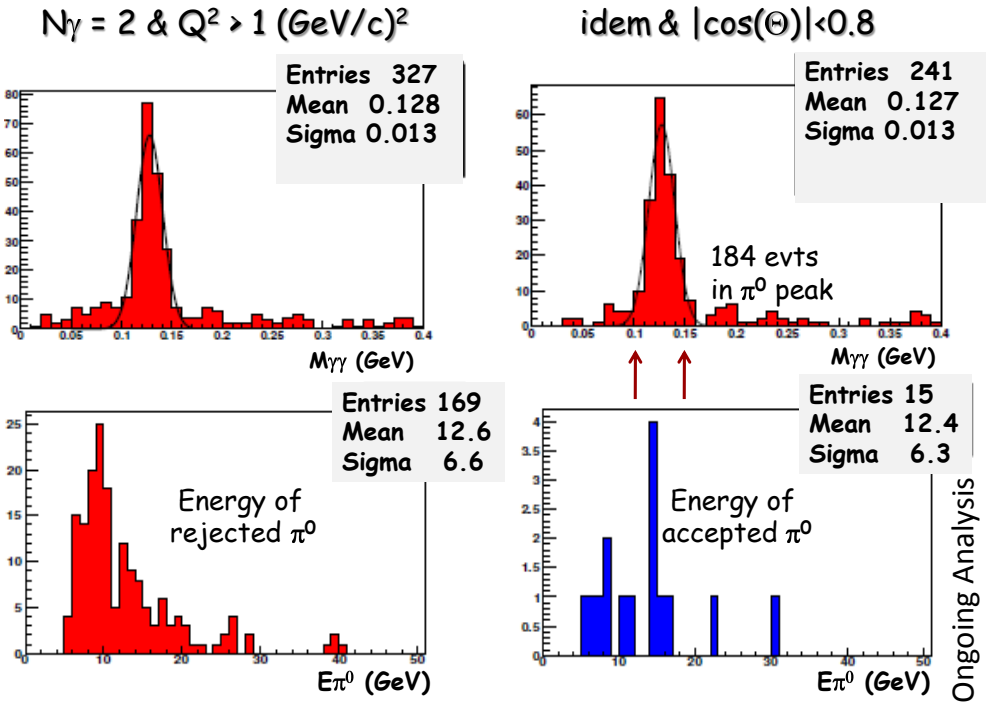


Figure 4: The $\pi^0$ signal for $2\gamma$ in ECAL1 selecting $Q^2 > 1$ (GeV/$c$)$^2$ events (top), also applying a $|\cos(\theta)| < 0.8$ cut. The energy of the $\pi^0$ for the rejected (169) and accepted (15) events by the DVCS analysis (bottom).

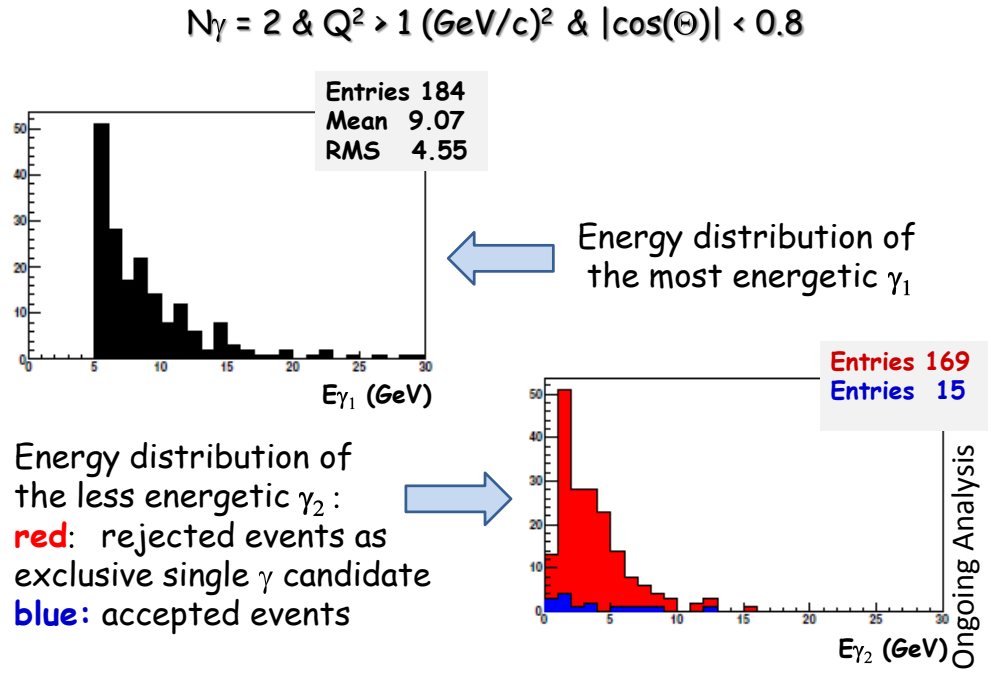


Figure 5: The energy distribution of the most energetic photon $\gamma_1$ for the 184 selected $\pi^0$ events (top left). The energy distribution of the less energetic photon $\gamma_2$ (bottom right), events rejected as exclusive single $\gamma$ candidate (red), accepted events (blue).

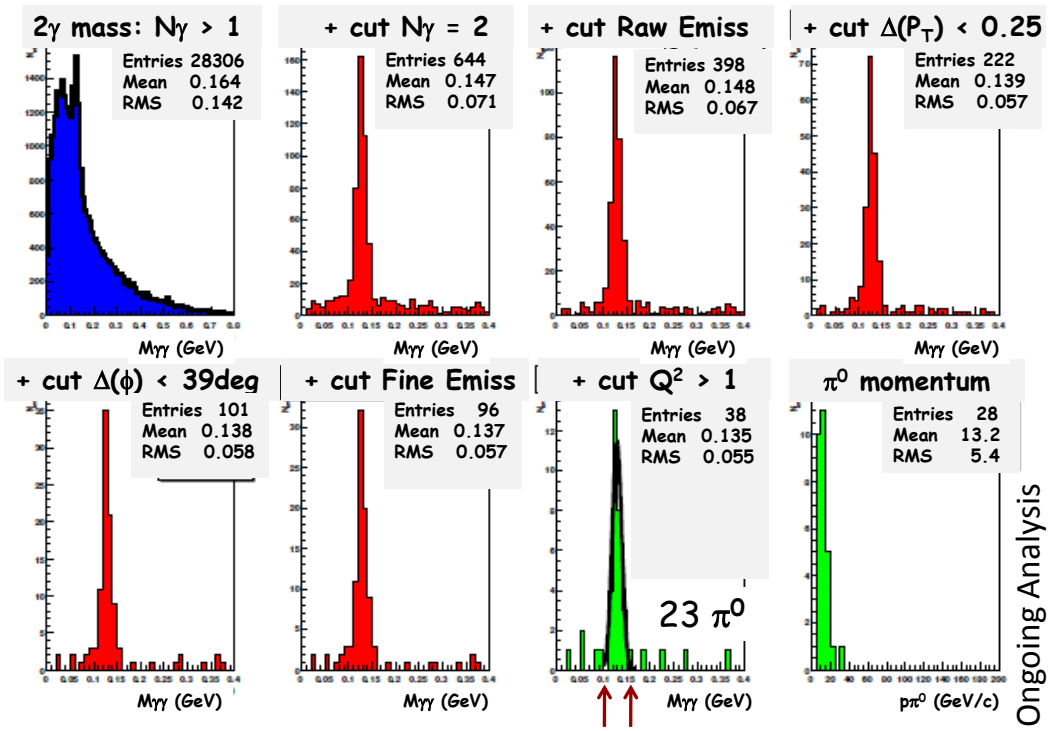


Figure 6: The $\pi^0$ signal applying exclusivity cuts step by step. The last two plots show the exclusive $\pi^0$ mass and momentum distributions.

the 169 rejected events and the same distribution for the 15 events passing the DVCS exclusivity cut. Releasing the $Q^2 > 1$ $(\mathrm{GeV}/c)^2$ cut leads to 351 $\pi^0$ candidates out of which the same 15 events remain as DVCS candidates.
The energy distributions of the corresponding high energy photon $\gamma_1$ and of the low energy photon $\gamma_2$ (assumed undetected) is shown in Fig. 5.
In a second step we have tried to estimate the yield of exclusive $\pi^0$ events. A set of exclusivity cuts, as for DVCS but tuned to $\pi^0$, has been applied on the missing energy $E_{\mathrm{miss}}$, the transverse missing-momentum balance $\Delta p_T = |p_{T\mathrm{miss}}| - |p_{T\mathrm{rpd}}|$, the difference $\Delta\phi = |\phi_{\mathrm{miss}} - \phi_{\mathrm{rpd}}|$ between the azimuthal angle of the missing momentum $\phi_{\mathrm{miss}}$ and the azimuthal angle of the proton candidate $\phi_{\mathrm{rpd}}$. Figure 6 illustrates the reduction of the $\pi^0$ yield after applying each cut.
Figure 7 shows the $\cos(\theta)$ distribution for both $\pi^0$ and background events. Also shown is a properly normalised ratio of the two distributions (signal/background). It indicates that the phase space close to $\cos(\theta) = \pm 1$ is more populated by background events.
Figure 8 shows the same distribution after applying the $Q^2 > 1$ $(\mathrm{GeV}/c)^2$ cut. It displays for the (almost) pure $\pi^0$ sample a flat distribution, as expected from the decay of the pseudo-scalar $\pi^0$. Figure 9 shows the $\pi^0$ mass and momentum distribution in 3 $x_{Bj}$ bins for the same sample.
Assuming that only the high energy photon $\gamma_1$ is detected, the 23 events are analysed as valid DVCS candidates. Figure 10 shows that only 11 events survive the DVCS selection. Note that the rejection concerns primarily events for which the energy of the undetected photon $E_{\gamma_2}$ is above 2 GeV. The 11 non-rejected events are a subset of the non-rejected 15 events obtained from the $\pi^0$ sample with no exclusivity cuts. We conclude that the prob-

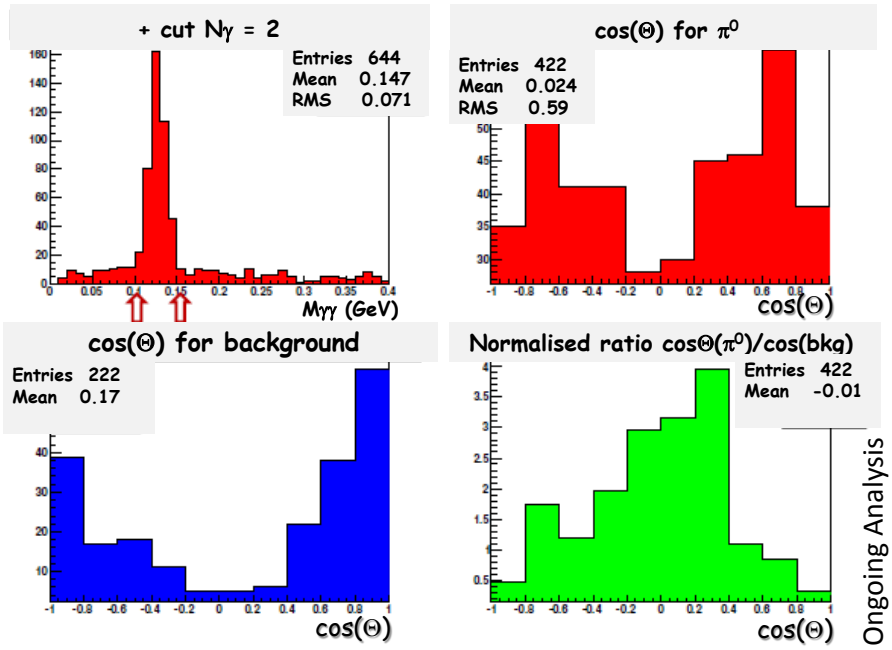


Figure 7: The $\cos(\theta)$ of one $\gamma$ calculated in the decaying $\pi^0$ centre of mass shown for signal and background events. Also shown is the normalised ratio of the two distributions vs $\cos(\theta)$.

ability for the non-exclusive $\pi^0$ events to generate background contamination to DVCS is small.
Note that the material presented here was fully cross-checked [14]. However, the result is still preliminary and we will soon start a new production of the 2009 DVCS data with much improved ECALs calibration and software which will provide us with more precise numbers.
A more quantitative answer to the Referees' question can only be obtained with Monte Carlo simulations. A first estimate was provided very recently [18]. From 100 generated $\pi^0$s about 50 are reconstructed (with their large majority detected in ECAL1) having an energy distribution that is roughly compatible with the above shown distribution of measured events. Among the 50 non-reconstructed $\pi^0$s, about 40 have only one photon detected and are therefore candidates to generate DVCS background. Combining these numbers with the above background estimate from reconstructed $\pi^0$s, one gets $15 \times \frac{40}{50} = 12$ background events. The exclusivity cuts used in this analysis are broad and we are confident that they can be optimised, leading to a more efficient $\pi^0$ background rejection. We consider therefore this number as an upper limit of the $\pi^0$ contribution to the sample of about 44 DVCS candidate events seen in the $x_{Bj} > 0.03$ bin [17].

**Q 4:** *p 19: 4.6 10**8 muons/spill seems optimistic, machine seems to be able to promise only 4.0.*

A: Indeed, the presently safely reachable flux is $4 \times 10^8$ muons for a spill of 9.6 s length. The $4.6 \times 10^8$ came from simply doubling the achieved flux for a 4.8 s spill with $1.4 \times 10^{13}$ protons on the primary T6 target in the M2 beam line. The difference of 15% is not very

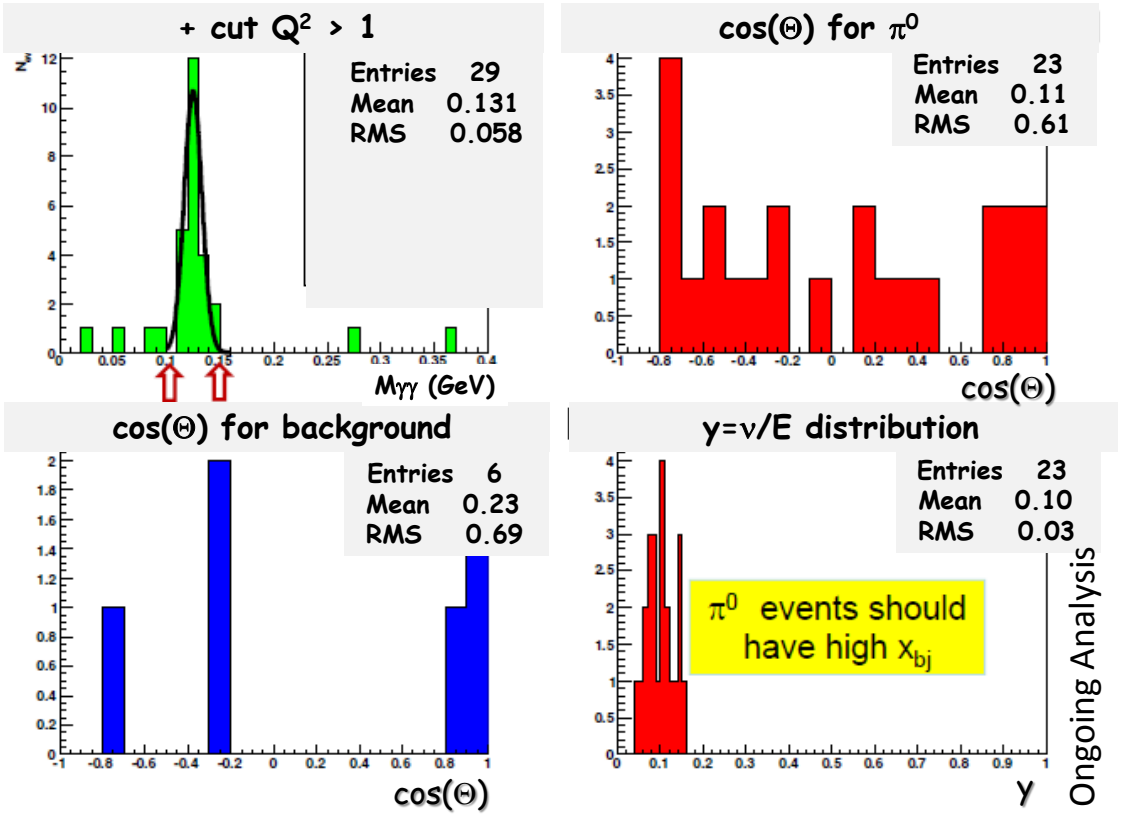


Figure 8: The $\cos(\theta)$ of one $\gamma$ calculated in the centre-of-mass system of the decaying $\pi^0$, shown for signal and background events for $Q^2 > 1$ $(\mathrm{GeV}/c)^2$. The $\pi^0$ candidate events have low values ($\sim 0.1$) of $y = \nu/E$ therefore are expected to have high $x_{Bj}$.

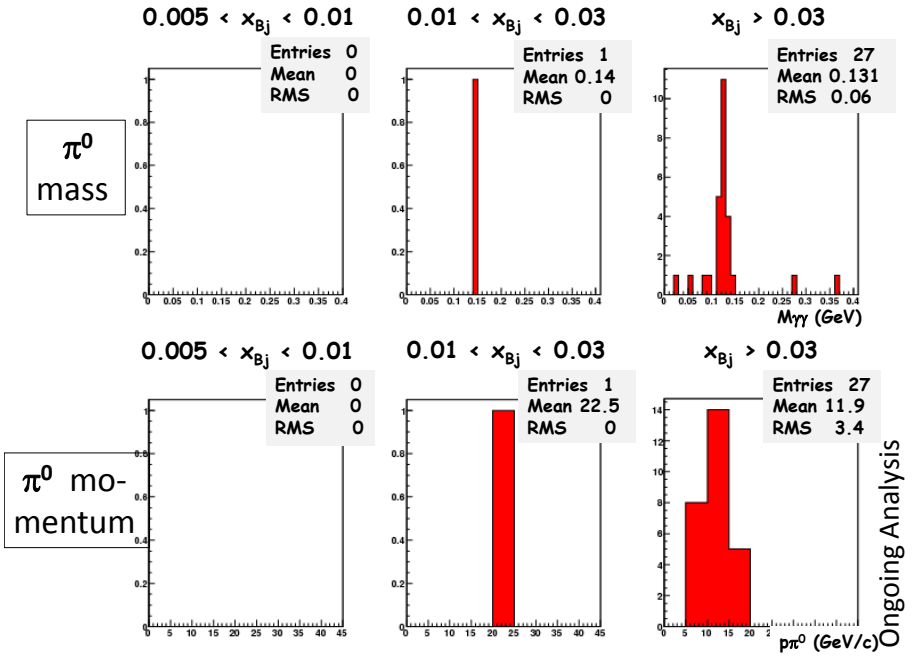


Figure 9: The mass and momentum distribution of the $\pi^0$ candidates in 3 $x_{Bj}$ bins (as used for the DVCS analysis).

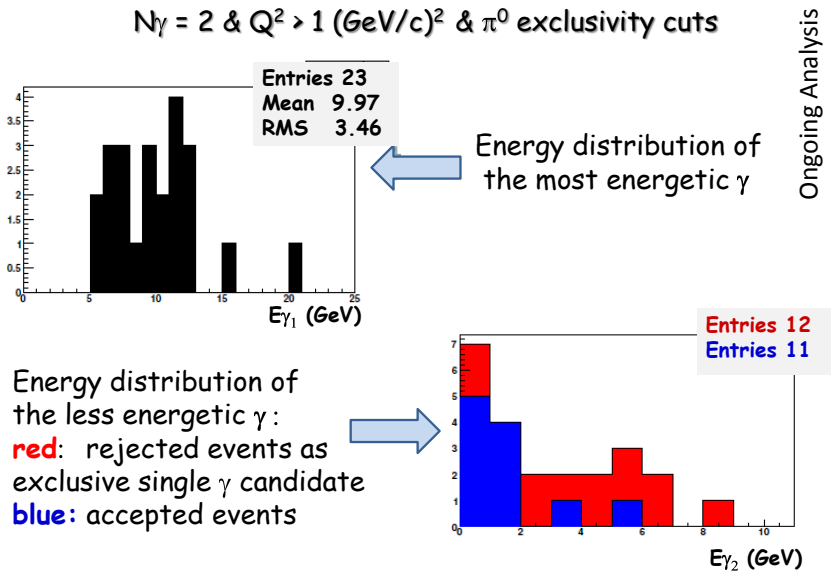


Figure 10: The energy distribution of the most energetic photon $\gamma_1$ for the 23 selected exclusive $\pi^0$ events (top left). The energy distribution of the less energetic photon $\gamma_2$ (bottom right): events rejected as exclusive single-$\gamma$ candidate (red), events accepted (blue).

large but still we plan to follow up the issue in discussions with the accelerator group in order to better understand it and possibly be able to remove the additional limitations for the long spill. Recently, the SPS has delivered up to $2.7 \times 10^{13}$ protons in a 9.6 s spill. This is only 4% below the assumed intensity.

**Q 5:** *p 19: it is mentioned that the analysis is done in 2-dimensions in t and phi, for what is it important?*

A: The DVCS cross-section $\mathrm{d}^4\sigma/\mathrm{d}Q^2\mathrm{d}x_B\mathrm{d}t\,\mathrm{d}\phi$ depends on the four variables $x_B$, $Q^2$, $t$ and $\phi$. The expected statistics will allow a multi-dimensional study in the following binning:

- 6 bins in $x_B$ $[0.005; 0.01]$, $[0.01; 0.02]$, $[0.02; 0.03]$, $[0.03; 0.07]$, $[0.07; 0.13]$, $[0.13; 0.27]$
- 3 bins in $Q^2$ [1; 2], [2; 4], [4; 8] GeV$^{-2}$
- 6 bins in $t$ from 0.06 to 0.7 GeV$^{-2}$
- 20 bins in $\Phi$ in the complete range $[-\pi; +\pi]$.

For the $t$-slope determination, an integration over $\phi$ has to be performed in order to get rid of the interference term and to keep only the pure DVCS contribution, which is represented mainly by the term $c_0^{DVCS}$ (see *Eq. 6, p. 15*). The $t$-dependence of the cross-section is studied over the six bins shown above. The result is presented for the five highest bins in $x_B$ integrated over their range in $Q^2$ (see *Fig. 6, p. 21*). We note that the larger statistics expected for exclusive $\rho$ production allows one to present the results also in dependence on $Q^2$ using the three bins shown above (see *Fig. 12, p. 28*).
For the determination of the real part of the Compton form factor $\mathcal{H}$ the azimuthal dependence of the cross-section, *i.e.* its dependence on $\phi$, must be exploited in order to be able to extract the coefficients $c_0^I$ and $c_1^I$ (see *Eq. 10, p. 16*). *Figure 10* on *p. 26* and *Fig. 11* on *p. 27* show the $\phi$ dependence of the cross-section for 12 bins in $(x_B, Q^2)$ integrated

over the $t$ range. *Figure 9* on *p. 24* represents the $\cos\phi$ modulation of the asymmetry for 6 bins in $x_B$ and 6 bins in $t$, integrated over the $Q^2$ range.

**Q 6:** *p 22: How strong is the "indication" that the factorized ansatz is disfavoured? What is the relevance of the* COMPASS *measurement if it is not the case (figure 7)?*

A: GPDs depend upon three kinematic variables: $t = -\Delta_L^2 - \Delta_T^2$, the four-momentum squared transferred between initial and final nucleon states as well as $x$ and $\xi \simeq x_B/(2 - x_B)$, average and half the difference between the initial and final longitudinal momentum fractions of the nucleon carried by the partons throughout the process (note that $x$ is not accessible in DVCS).
For GPDs, "factorised" ansatz means that the $t$ dependence of the GPD is completely uncorrelated with the $(x, \xi)$ dependence

$$H^f(x, \xi, t) = h^f(x, \xi) \cdot F_1^f(t)$$

where $h^f(x, \xi)$ is related to a quark distribution function and $F_1^f(t)$ is a form factor. This very simple model was elaborated at an earlier stage. It had the advantage to reproduce all the boundary conditions of GPDs and to give a first idea for predictions of the contributions for hard exclusive processes (cf. first VGG calculations in 1998–99: Refs. [19] and [51]).
The four-momentum transfer $t$ is conjugate to the impact parameter $b_\perp$ (*i.e.* the transverse distance of the active parton to the centre of momentum of the nucleon), as can be seen from *Eq. 3, p. 10*

$$q^f(x, b_\perp) = \int \frac{\mathrm{d}^2\Delta_\perp}{(2\pi)^2} e^{-i\Delta_\perp \cdot b_\perp} H^f(x, 0, -\Delta_\perp^2).$$

The choice of $b_\perp$ is motivated by simple physical ideas. Partons with small $x$ can be considered to arise from a cascade of branching processes, sometimes called "Gribov diffusion". This sort of processes leads intuitively to a mean-squared impact parameter $\langle b_\perp^2 \rangle$ growing at small $x$ as $\log(1/x)$. We expect a corresponding interplay between longitudinal momentum and transverse position degrees of freedom in the nucleon, called 'nucleon tomography', as it is presented in the sketch of *Fig. 2, p. 10*. This behaviour is provided by the 'Regge-motivated' form for GPDs

$$\begin{aligned} H^f(x, 0, t) \simeq q_f(x) \exp\left(\frac{1}{4}\langle b_\perp^2 \rangle t\right) &\simeq q_f(x) \exp\left(\frac{1}{2} B(x) t\right) \\ &= q_f(x) \exp\left(\left(\frac{1}{2} B_0 + \alpha' \log(\frac{1}{x})\right) t\right) \end{aligned}$$

where $q_f(x)$ is the PDF for the given parton species $f$. Note that a large value of $\alpha'$ corresponds to a $t$ dependence which is highly correlated with $x$, in which case the 'factorised' ansatz is disfavoured, while a small value of $\alpha'$ implies a small or vanishing correlation.
We give below a summary of the main experimental and theoretical facts on the knowledge of $B$ and $\alpha'$. This was already discussed in *Sect. 1.1, pp. 10–11* and in *Sect. 1.3.1, p. 20*, where also impact parameter $b_\perp$ and transverse radius $r_\perp$ (*i.e.* the transverse distance of the active parton to the centre of momentum of the spectator system), were introduced. The quantities $b_\perp$ and $B(x)$, related to the GPD at $\xi = 0$, are not accessible experimentally but can be evaluated in lattice calculations. The quantities $r_\perp$ and $B(x_B)$, related to the

GPD at $x = \xi$, can be accessed experimentally using the above given relation between $\xi$ and $x_B$. At small $x_B$, they can be measured through the pure DVCS amplitude which is predominantly imaginary.
At small $x_B$, the H1 and ZEUS experiments (*Refs. [18, 53, 54]*) did not observe a change of the $t$-slope $B(x_B)$ of the DVCS cross-section for $x_B$ ranging between $10^{-4}$ and $10^{-2}$, which led to the conclusion of a value of $\alpha'$ close to zero. This allowed the determination of the average transverse proton radius $\langle r_\perp \rangle$ to be $0.65 \pm 0.02$ fm in the HERA kinematics. This value turns out to be exactly equal to the transverse charge radius of the proton which is given by $\sqrt{2/3}\langle r_{charge} \rangle$ where $\langle r_{charge} \rangle = 0.8$ fm. Here, the factor 2/3 enters as form factors (FF) are defined in 3-dimensional space ($\langle r^2_{charge} \rangle = 6\, \mathrm{d}\log(FF)/\mathrm{d}t$), while now we are considering the projections in the transverse plane ($\langle b^2_\perp \rangle = 4\, \mathrm{d}\log(GPD)/\mathrm{d}t$).
It may be interesting to note that from measurements of $J/\psi$ production at H1 with $Q^2$ ranging from 2 to 80 GeV$^2$ [20] also a small value $\alpha' = 0.019 \pm 0.139 \pm 0.076$ GeV$^{-2}$ was obtained which is significantly smaller than the value $\alpha' = 0.25$ GeV$^{-2}$ known to describe the 'soft Pomeron'.
At large $x_B$ ($\geq 0.2$), there exists no direct experimental determination of $B(x_B)$ or $\alpha'$ by neither HERMES or JLab, because in these kinematics the pure DVCS contribution is always dominated by a large contribution of the DVCS–Bethe-Heitler interference term. The only information here comes from fits adjusted to form-factor data, which give a large value of $\alpha'$ close to 1 GeV$^{-2}$ for valence quarks (*Refs. [55, 56]*). Such a large value of $\alpha'$ is remarkably close to the slope parameter for meson Regge trajectories in hadronic collisions.
Another indication that the factorised ansatz is disfavoured at large $x$ comes from lattice calculations *[12]*. The average value of $b_\perp(x)$ was found decreasing from about 0.4 fm to 0.2 fm for typical values of the longitudinal momentum fraction $x$ increasing from 0.2 to 0.4.
Altogether, experimental information on the degree of the correlation between $(x, \xi)$ and $t$ is still quite poor, so that its measurement in the uncharted $x_B$ region provided by COMPASS is essential to elucidate the issue of 'nucleon tomography', thereby also constraining GPD fits. This will be made possible by exploiting two specific features of the CERN M2 muon beam used by the COMPASS experiment:

1. At the high energy of the muon beam, the pure DVCS cross-section can be measured, more specifically the $x_B$ dependence of its $t$-slope. This will be used to determine the parameters $B(x_B)$ and $\alpha'$ without any model. (see *Sect. 1.3.1, Fig. 6, p 21*).
2. From data to be taken with both the positive and negative highly-polarised muon beams the Beam Charge and Spin Difference of the DVCS cross-sections will be determined. This opens access to the real part of the Compton form factor, which is predominantly related to the GPD $H$. (see *Sect. 1.3.2* and *Figs. 7–11, pp. 21–27*). This measurement will allow constraining GPD models and global GPD fits.

**Q 7:** *p 35 bottom: what is the outcome of the 2009 run about limitations of absolute normalisation?*

A: We recall that the principal goal of the 2009 DVCS test run (cf. *p. 34*) was "to provide a first evaluation of the relative contributions of the $|DVCS|^2$ and $|BH|^2$ terms...", which was achieved. The COMPASS-II programme does require to reach a level of accuracy of a few percent in the determination of cross-sections. As discussed below, a standard of 10%

or better has been reached for absolute measurements from data taken in previous years, which were not meant for such a precision.
A precise evaluation of cross-sections is not required, a priori, for spin asymmetry measurements. However, a determination of the cross-section for muoproduction processes on the $^6$LiD (polarised) target has been performed to check the validity of the QCD models used to extract the gluon polarisation $\Delta G/G$. Recently, a precise evaluation of the semi-inclusive low-$Q^2$ muoproduction cross-section $\mathrm{d}\sigma/\mathrm{d}p_T$ of a charged hadron with transverse momentum $p_T$ was achieved using the 2004 data. One important outcome of these studies is a determination of the $F_2^d$ structure function from inclusive events [21]. The comparison with world data confirms that a standard of accuracy of 10% or better has been reached for absolute cross-sections derived from the present data. A very detailed analysis of luminosity was performed for part of the 2004 data which we summarise in the following.

Spill-by-spill luminosity: One defines an effective, integrated luminosity $L$ (recorded luminosity) for each spill as the instantaneous luminosity $\mathcal{L}$ reduced by the relative dead times of the DAQ ($d_{\mathrm{daq}}$) and trigger veto ($d_{\mathrm{veto}}$) systems

$$L = \int_{t_1}^{t_2} \mathcal{L}(t)\,(1 - d_{\mathrm{daq}}(t))\,(1 - d_{\mathrm{veto}}(t))\,\mathrm{d}t.$$

The beam intensity varies within a spill and from spill to spill. The above definition of $L$ takes into account the strong correlation of beam intensity with the DAQ and veto dead times.

Good spill selection: A standard procedure in the muon programme is to use so-called Bad Spill Lists (BSL). Spills are marked as "bad" if they fall below their neighbouring spills in one of the three figures of merit:

- the average number of primary vertices per reconstructed event,
- the average number of tracks in the primary vertex,
- the average number of beam tracks per reconstructed event.

In the analysis reported here, an additional figure of merit was introduced for each spill. This so-called Event Number Ratio (ENR) is defined as the number of reconstructed events divided by the number of physics triggers. Variations of this quantity were shown to be correlated to hardware problems and also to accidental loss of events during data production. Therefore an additional rejection of spills on the basis of the ENR has been applied. Figure 11 (left) shows the resulting distribution of ENR values averaged per run. The width of the distribution of 1.8% provides an estimate of the systematic uncertainty for the COMPASS reconstruction efficiency.

SPS spill structure and selection within the spill: The SPS provides an extracted beam whose intensity is rising at the beginning of a spill and then becomes stable. In addition, the beam can be poorly debunched at the beginning of a spill. For a precise luminosity and an absolute cross-section determination, the part of the spill is selected where intensity is close to the maximum as illustrated in Fig. 11 (right). This defines the analysed time interval $[t_1, t_2]$ for a particular spill.

Effective beam flux determination: The integrated beam flux is determined by a scaler connected to a beam counter (FI02) and providing the rate $R_{\mathrm{sc}}$. Since not all beam

Event Number Ratio  Beam Flat Top selection

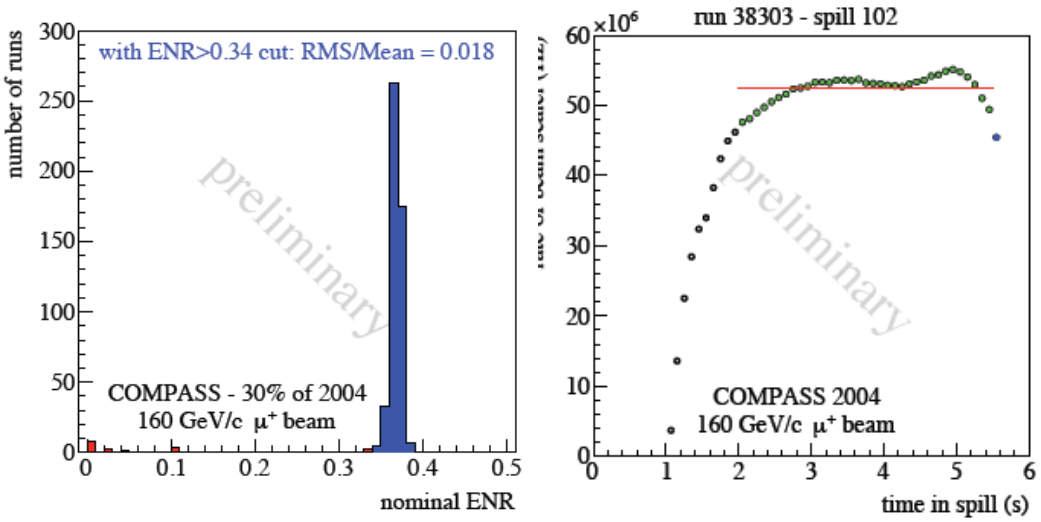


Figure 11: Left: distribution of nominal values of ENR, the (blue) peak shows the runs with an ENR value above the chosen hard-cut threshold of 0.34, the (red) areas left of this cut show the runs rejected. Right: an example of spill structure, the (green) filled points indicate time bins used for the analysis starting at $t_1 = 2$ s. The (blue) open points indicate bins which are excluded by a $t_2 = 5.5$ s in this case.

particles seen by FI02 cross the target, the quantity $R_{\rm sc}$ is not equal to the real beam flux $R_{\rm beam}$. The latter is calculated from the number $N_{\rm rt}$ of random triggers and the number $N_{\rm bt}$ of reconstructed beam tracks in the random-trigger events passing through the entire target cells

$$R_{\rm beam} = \frac{N_{\rm bt}}{\Delta t\, N_{\rm rt}}$$

with the random-trigger gate width $\Delta t$. With the $^6$LiD target, the ratio $R_{\rm beam}/R_{\rm sc}$ is about 0.65 with an systematic uncertainty of $\sim 5\%$. This is the dominant systematic error in the determination of luminosity. Studies of variation of this ratio with beam intensity have shown that inherent limitations of the scaler system is the origin of this uncertainty. The precise measurement of beam flux will not rely on this scaler value $R_{\rm sc}$ but be derived from $R_{\rm beam}$, the number of reconstructed beam tracks sampled by a random trigger. The required $N_{\rm rt}$ per spill and the optimum $\Delta t$ to provide sufficient statistics need to be optimised. All the tools have been developed and are fully available to provide a reduction of the systematic error on beam flux by a factor of 2 to 3 from the above quoted value of 5%.

DAQ dead time determination: The DAQ dead time is defined as the fraction of data taking time in which triggers cannot be accepted because the DAQ is busy acquiring and recording the previously triggered events. It is measured directly in COMPASS by counting the number of trigger attempts and the number of accepted trigger attempts with scalers that are written to each recorded event. It was demonstrated that the DAQ lifetime correction has a negligible systematic error.

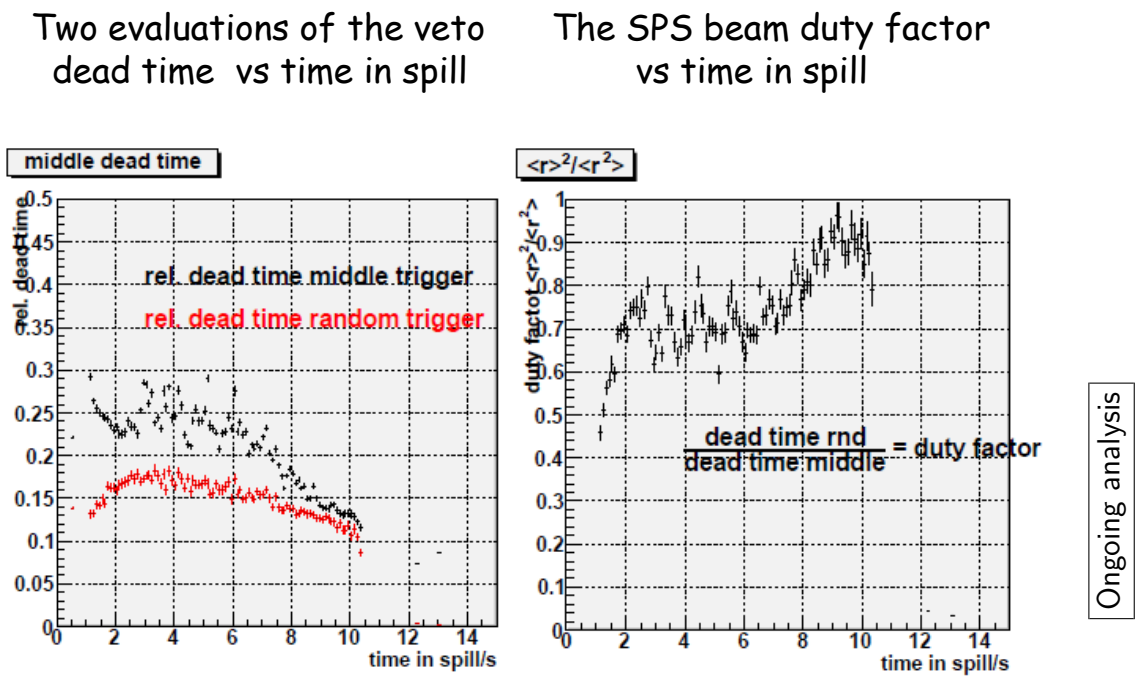


Figure 12: Left: the dead time of the middle trigger and the random trigger vs. time in spill. Right: the SPS beam duty factor vs. time in spill.

Veto dead time determination: A large fraction of halo muons will cause unwanted triggers, if not rejected by the veto system (see *p. 86*). The dead time of the full veto applied to inclusive triggers is presently $\sim 20\%$ at nominal beam intensity for a well debunched beam. The DVCS measurements involve data taking with both $\mu^+$ and $\mu^-$ beam with an available $\mu^-$ beam intensity of about 1/3 of the $\mu^+$ intensity. Combination of these data will require an excellent control and understanding of the dependence of dead time (including other potential intensity-dependent loss factors) with varying beam intensity and duty factor.
The following method is presently applied [22]:

- determine the dead time as a function of time in spill,
- extract the beam duty factor, thereby allowing its online monitoring,
- determine the effective width of the veto anti-coincidences.

Shown in Fig. 12 (left) are two evaluations of the veto dead time, one for the middle trigger, the other for the random trigger. The significant difference between the two dead times which tends to drop with time in spill is a clear indication that the delivered beam has a non-uniform time structure. Figure 12 (right) shows an estimate of the beam duty factor as a function of time in spill. The projected reduction foreseen in the proposal by a factor of 2 of the veto dead time (see answer to question 16) will contribute to reduce the systematic error on event losses due to dead time. More studies are needed on available data, including the DVCS test data, to quote a realistic systematic error on veto dead time measurements.

Systematic error and prospects for absolute cross-sections: The present status of the contributions to systematics for absolute measurements and prospects for improvements is:

- 1.8% from the left-over variation of the reconstruction efficiency after appropriate cuts on the ENR distribution.

- 5% from the beam flux determination which can be reduced by a factor of 2 to 3.
- a negligible contribution from the DAQ dead time.
- The veto dead time is presently of the order of 20–25% at nominal $\mu$ beam intensity. There is no definite estimate of the systematic error on this quantity. However, a reduction of dead time by a factor of 2 is envisaged. An online monitoring of the beam duty cycle and also the trigger dead time versus the time in spill is available. It will contribute to reducing the errors on the determination of losses from veto dead time which could lead to charge-dependent systematic errors due to the different intensities of $\mu^+$ and $\mu^-$ beams.
- A specific item for DVCS studies is the control of the amount of target material which for the case of the long (2.5 m) Liquid Hydrogen (LH) target has led to strict specifications for control and stability of the LH target density at 3% level. Note that, contrary to the error from dead time, the error on density should not depend on beam intensity and only affects the absolute normalisation of cross-sections and by the same amount their sum and difference.

Conclusion: We have not yet reached the envisaged necessary few-percent level in the systematic error in the determination of luminosity. However, the above figures demonstrate that this can be achieved. The required tools have been developed and are available. Work is ongoing analysing existing data, including the 2009 DVCS test data, with the goal to confirm the ultimate precision for the determination of absolute cross-sections.

**Q 8:** *Section 2.1.1 What is the result of the strange quark measurement with the LiD target? Can such a measurement be done with the DVCS test data taken in 2009?*

A: The extraction of the strange quark distribution function $s(x)$ and the quark fragmentation functions (FFs) is based on the measurement of identified hadron multiplicities. The determination of hadron multiplicities requires the knowledge of the absolute acceptance of the spectrometer with a precision of a few percent. Such a precision is needed for the first time in Compass, since only spin asymmetries of cross-sections had been studied so far, where these effects cancel at first order. Although the Compass setup was not designed originally for such absolute measurements, we think that we can achieve the necessary accuracy.
Work has started on the 2004 data for which the MC analysis software is thought to be well under control. A full MC chain has been developed to calculate an absolute overall acceptance, which includes all known contributions: acceptance and efficiency for muons and hadrons, particle identification performance (efficiency and misidentification) for pions and kaons as well as smearing effects and radiative corrections. The acceptance was computed in a 2-dimensional space using the variables $x$ (Bjorken-$x$) and the fraction $z$ of the virtual-photon energy carried by the hadron. For the RICH, it was finally decided to use performance tables based on data as described below, rather than a pure MC description. The result of the overall acceptance for SIDIS events with $K^+$ and $\pi^+$ is shown in Fig. 13 for the full coverage of the spectrometer in 12 $x$ bins and 4 $z$ bins.
For kaon identification, the performance of the RICH detector is crucial. Kaons from $\phi$ decays on one hand and pions from $K_S$ decays on the other permit us to determine the RICH tables of performances. They contain the efficiency as well as the probability

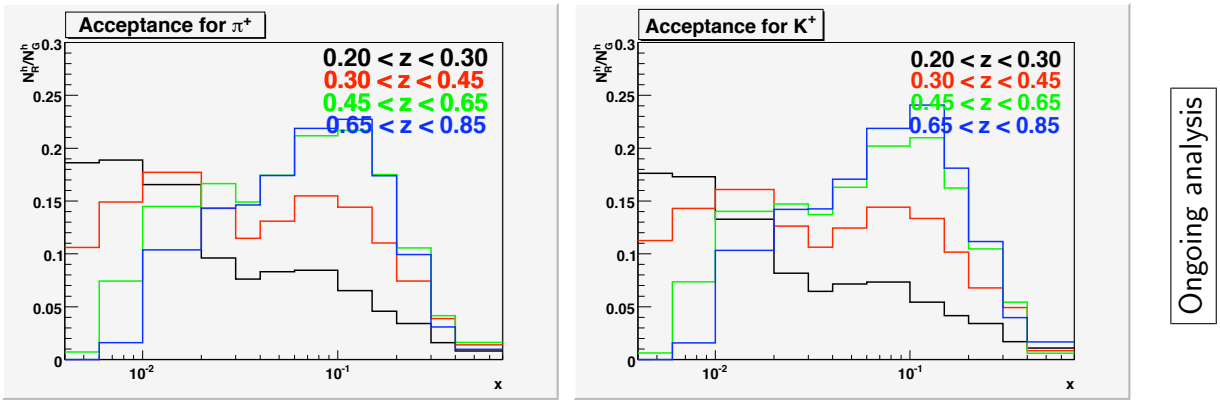


Figure 13: Overall acceptance of the spectrometer for SIDIS events with identified $\pi^+$ (left) and $K^+$ (right) for 12 $x$ bins and 4 $z$ bins, calculated from MC for the 2004 setup, data are from periods W28 to W31.

of misidentification of all particles and are produced as a function of two variables, the angle at the RICH entrance and the momentum of the particle, a choice which is well matched to the problem. The tables are used as input to the MC. Just as an illustration of the possible size of the effect on multiplicities, we show in Fig. 14 the corresponding values, efficiency and probability of misidentification of pions and kaons by the RICH as a function of $x$. For historical reasons, only the first 10 $x$ bins appear in the figure. We observe in Fig. 14 that the performances of the RICH are similar for pions and kaons. This is in agreement with Fig. 13 where the large structures in the acceptance distributions were similar for $\pi^+$ and $K^+$. The RICH performance tables were built using the full 2004 statistics. They are used in the MC description of the spectrometer which applies to 4 periods only.

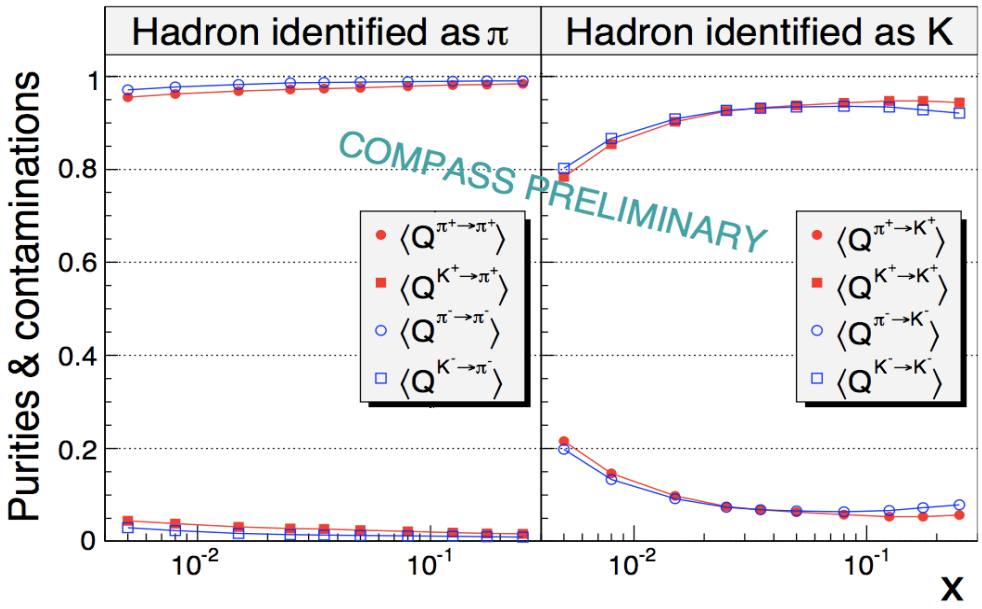


Figure 14: Efficiency and probability of misidentification of pions and kaons by the RICH for the full year 2004 corresponding to the 10 first $x$ bins of Fig. 13.

Note that the probability of misidentification of pions as kaons should be determined with very high accuracy, since pions are 5 times more abundant than kaons. In order to keep the misidentification low for both pions and kaons, in a first step we can determine the hadron multiplicities only in the region $x > 10^{-2}$. This approximately corresponds to keeping only particles with momenta below about 35 GeV/c, while above this value the purity of the RICH identification starts to decrease.

Up to now, 4 weeks of data were analysed, corresponding to about 1/3 of the 2004 data. They were chosen because the data were produced with the latest and best version of the COMPASS reconstruction program CORAL. Raw multiplicities for pions and kaons, which are defined as the number of pions and kaons per DIS event, were extracted. Then the acceptance correction was applied as calculated from MC following the procedure described above. It includes smearing effects in both $x$ and $z$ as well as radiative corrections. Results for the corrected multiplicities are shown in Fig. 15 as a function of $x$ for 4 $z$ bins. The upper lines with higher multiplicities correspond to the lowest $z$ bin, $0.2 < z < 0.3$.
The statistics shown corresponds to a total of 100 000 kaons, obtained in one period of one week with the 1.2 m LiD target. Work is still ongoing and the systematic uncertainty associated with the acceptance determination, which is certainly larger than the statistical error, has not been evaluated yet. The data are compared to a calculation based on PDFs from the MRST parameterisation and on FFs from the DSS one. We observe that the data follow the parameterisation, at least for the 3 lowest $z$ bins. Let us recall that no external input is used in the analysis and also that the uncertainty on the parameterisation is not known.
In Figure 15 only 9 $x$ bins are left, the first ($x = 0.005$) and the last two ones ($x > 0.3$) were dropped for this preliminary analysis because of low acceptance of less than 5%. In addition, among the remaining 9 bins shown, the last 2 $x$ bins ($x > 0.15$) correspond to values of $Q^2$ larger than 10, for which at this stage of the analysis the MC does not perfectly describe the data. Hence they should be taken with care. This feature is not surprising since the acceptance shows a steep decrease at high $x$ (see Fig. 13), especially for high $z$ values. Finally, as explained above, if we want to consider only data for which the misidentification of pions into kaons is low, *e.g.* below 12%, we should reject in addition the first bin and keep only data with $x > 0.01$.
Once the pion and kaon multiplicities are determined, the next step is to disentangle the physics quantities involved, namely PDFs and FFs. The final goal of the proposed extensive measurement of hadron multiplicities as a function of several variables is to provide data as input for global NLO QCD fits where this separation will be done. A more restricted objective is the determination at leading order of the strange quark distribution. The $s(x)$ distribution can be extracted exploiting a simple formula that uses $K^+$ and/or $K^-$ multiplicities, assuming other PDFs ($u, \bar{u}, d, \bar{d}$) as well as FFs to be known from literature. The accuracy on the multiplicities will be determined mostly by the systematic uncertainty of the acceptance. In the equation giving the kaon multiplicity versus PDFs and FFs, the weight of the strange quark distribution function is only one half on average. As an illustration, we show the simplified equation for a deuteron target where $s(x)$ is given as a function of the $K^+$ multiplicity $M(x)$ and where the smallest contributions ($\bar{u}$, $\bar{d}$) were neglected:

$$s(x) = Q(x)\frac{5M(x) - 4D_2 - D_3}{D_1 + D_3 - 2M(x)}.$$

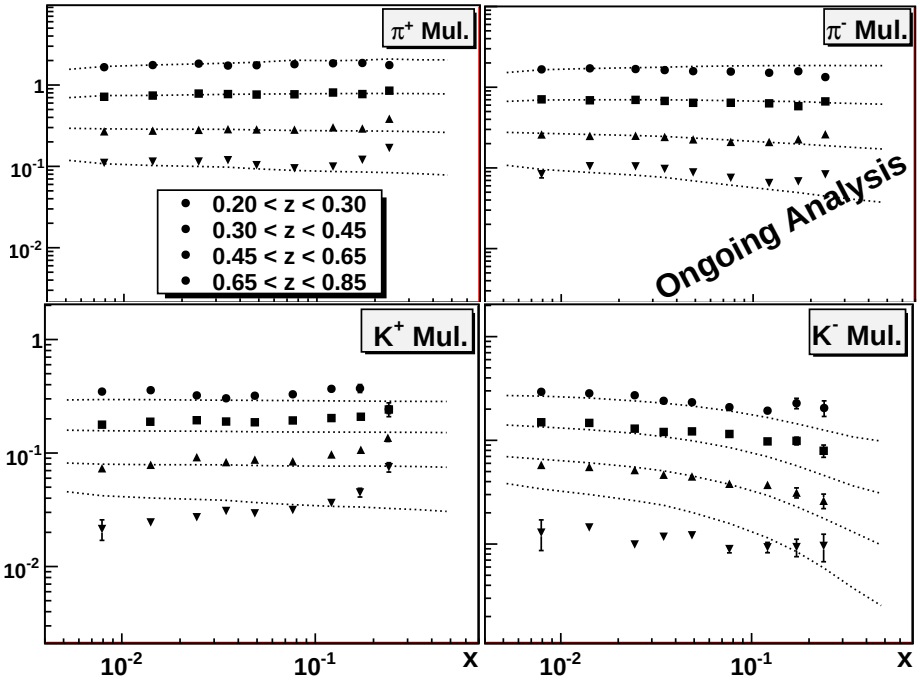


Figure 15: Multiplicities of pions and kaons corrected for spectrometer acceptance, shown as a function of $x$ for 4 $z$ bins. The upper lines (higher multiplicities) correspond to the lowest $z$ bin ($0.2 < z < 0.3$). 2004 data, 1 week, 1.2 m LiD target. The data are compared to a calculation using PDFs from the MRST parameterisation and FFs from the DSS one.

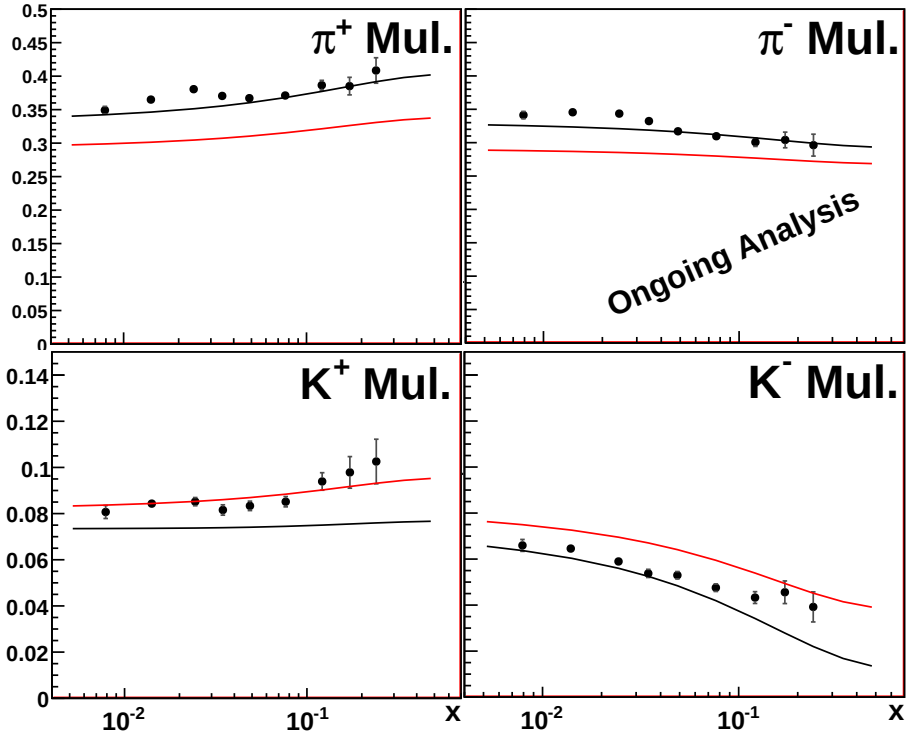


Figure 16: Multiplicities of pions and kaons as a function of $x$ integrated over $z$. Data are compared to calculations using two different sets of FFs, the DSS one (black curve) and the EMC one (red curve).

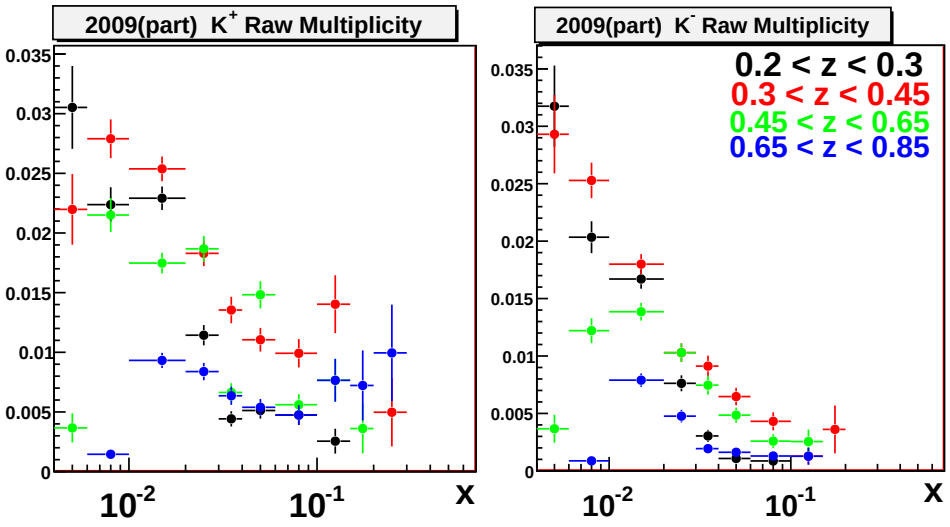


Figure 17: Raw multiplicities for $K^+$ and $K^-$, not corrected for acceptance, for 2009 LH2 test data ( 1/3 of statistics: 1500 $K^+$, 1000 $K^-$). Data are shown as a function of $x$, for 4 $z$ bins, inclusive triggers only.

In this equation $Q(x) = u(x) + d(x)$ and $D_1 = D_{\bar{s}}^{K^+}$, $D_2 = D_u^{K^+}$ and $D_3 = D_d^{K^+}$ are FFs integrated over $z$. As a result, if we can achieve an accuracy of the acceptance calculation of the order of 10% in this first study, it will propagate into an uncertainty of about 20% on $s(x)$ on average. Even with further improvements here, the dominant uncertainty will remain to be the poor knowledge of FFs. Hence for further improvement of the precision of the extraction of $s(x)$ an estimate of the kaon FFs is needed.
In Figure 16 we show the multiplicities integrated over $z$ and compare them to calculations using the PDFs from MRST together with two different sets of FFs, namely DSS and EMC, for which the FFs differ by factors of about 2. In order to be able to distinguish between them, the kaon multiplicities should be determined with an accuracy of about 5%. For this goal more work on MC and data stability is required.

In parallel about one third of the 2009 data taken during the DVCS test run with the $LH_2$ target has been processed, leading to a total of 1500 $K^+$ and 1000 $K^-$. The corresponding raw multiplicities, not corrected for acceptance, are shown in Fig. 17 for 4 $z$ bins. They also differ from raw 2004 data (not shown in this report) because the 2009 (polar angle) acceptance is larger. Once all 2009 data will have been analysed, we expect to get 7500 kaons in total. This can be compared to the 400000 kaons accumulated in the 4 periods analysed of the 2004 data. For these statistics, it will be possible to extract $s(x)$ in a limited $x$ range and only by assuming that FFs are known. Also the acceptance and efficiency of the spectrometer including the RICH performances for the 2009 setup will have to be studied.
However, a simple LO extraction of $s(x)$ assuming FFs known from literature is not satisfactory. We must recall that the final goal, as stated in the proposal, is an extensive measurement of hadron multiplicities in bins of $x, z, W^2$ or $Q^2$ and $p_t$ in order to be more independent from assumptions, in particular assumptions on FFs. Thus very high statistics are needed (as well as a good MC description of the apparatus). Also the same

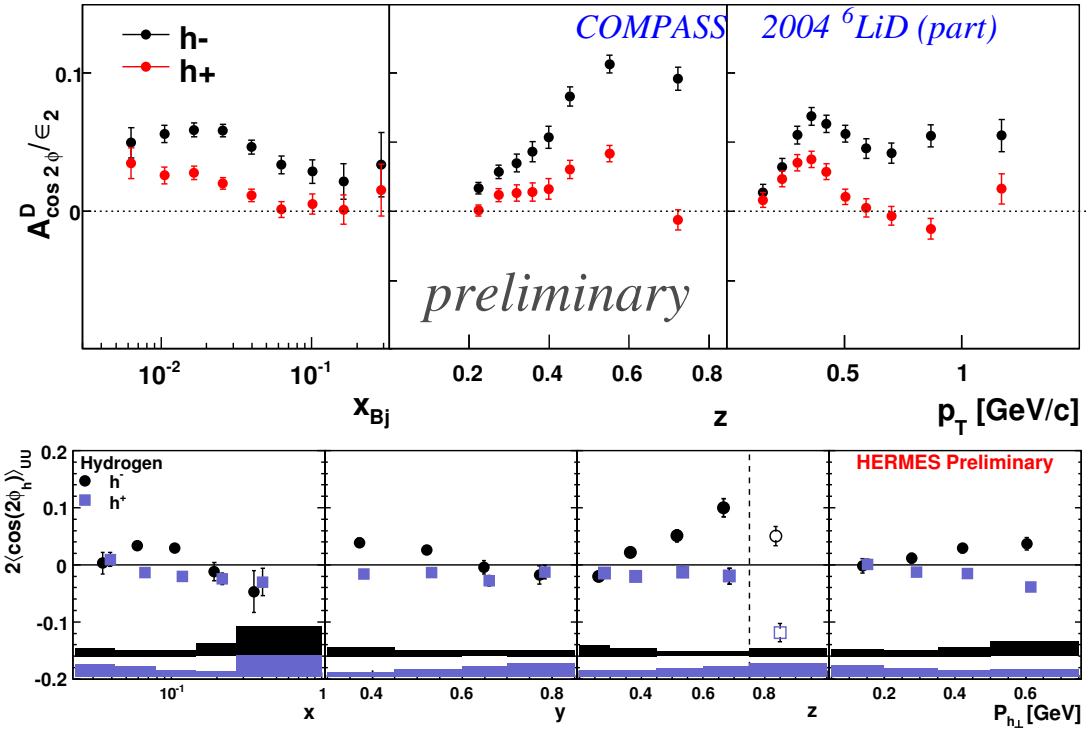


Figure 18: Preliminary results on the $\cos 2\phi$ azimuthal asymmetry for deuteron data from COMPASS (top) [23] and for proton data from HERMES [24] (bottom).

data will serve for measurements of various azimuthal asymmetries that are sensitive to TMDs, for which a binning in multiple variables is also important.

# Drell–Yan

**Q 9:** *p. 50 Was the Boer-Mulders already measured in DIS by* COMPASS*, or published by any other experiment?*

A: In SIDIS off unpolarised targets the Boer–Mulders function can be determined by measuring the amplitude of the $\cos 2\phi$ modulation in the azimuthal distribution of inclusively produced hadrons. This amplitude is in fact a convolution of the Boer–Mulders PDF with the Collins fragmentation function (FF). The latter can be extracted in global fits of the Collins asymmetry measured in SIDIS off transversely polarised targets and of azimuthal asymmetries measured in $e^+e^- \to$ hadrons. The existing HERMES, COMPASS and BELLE data already allowed for a first extraction of both the transversity distribution and the Collins FF [26]; more precise extractions are expected to become available in the not too distant future. Preliminary results on the $\cos 2\phi$ amplitude in unpolarised SIDIS were produced by COMPASS using deuteron data [23] and by HERMES using proton and deuteron data [24] (see Fig. 18). These data have been used for a first, model-dependent

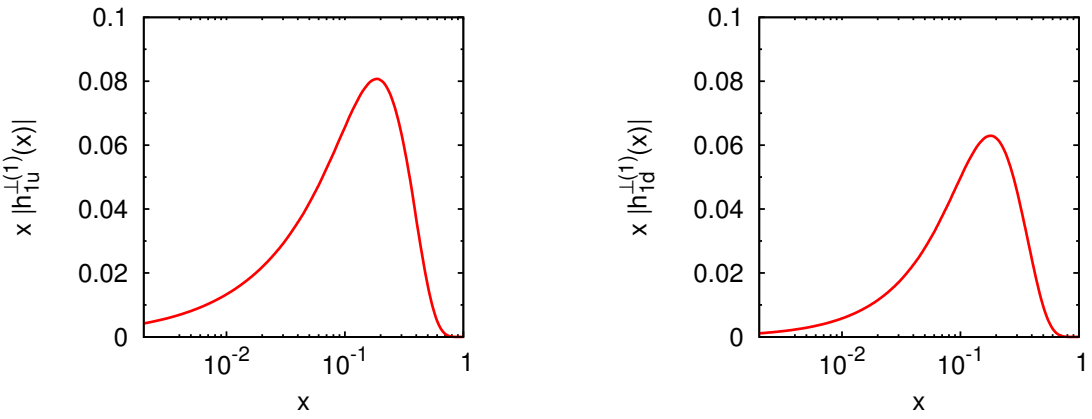


Figure 19: The $k_T$-integrated Boer–Mulders functions for $u$ (left) and $d$ quark (right) from the fit of the preliminary COMPASS and HERMES data [25].

extraction of the Boer–Mulders function shown in Fig. 19, which is presently available only without error bands [25].
In the future, expected improvements in the knowledge of the Collins FF and also more precise unpolarised SIDIS data will allow a better determination of the Boer–Mulders function. In particular, a new and more precise measurement of the $\cos 2\phi$ amplitude with a liquid hydrogen target is part of the COMPASS-II Proposal. It will be obtained as a by-product of the proposed DVCS measurement. Therefore, in the next few years, the knowledge on the Boer–Mulders function from SIDIS is expected to be at least satisfactory so that clearly its sign can be determined with high confidence.

**Q 10:** *Fig. 36 shows that the mean of the muons is 1 GeV, this seems to be good for TMDs, explain more*

A: Similar to SIDIS processes, also in Drell–Yan processes there exist two different scales, namely the dilepton mass $M(Q)$ and the dilepton transverse momentum $p_T$. For SIDIS processes, three distinct regions in transverse momentum $p_T$ were discussed in Ref. [27]. Correspondingly, for unpolarised Drell–Yan processes one can distinguish:

1. $p_T > Q \gg \Lambda_{QCD}$: large transverse dilepton momenta $p_T$ are produced mainly by hard gluon emission. Drell–Yan processes are well described by collinear, *i.e.* leading twist (twist-2), pQCD in next-to-leading order (NLO).
2. $\Lambda_{QCD} < p_T < Q$: the small-$p_T$ region is a typical 'non-perturbative' region. Small $p_T$ can be generated by the intrinsic motion of quarks in the colliding hadrons and/or by soft gluon emission. This is the region where the TMD formalism applies. Alternatively, unpolarised Drell–Yan data can also be described by collinear QCD plus soft gluon resummation, *i.e.* by (next-to-) next-to-leading log corrections.
3. $p_T \approx Q$: this is the intermediate region where $p_T$ is mainly generated by soft gluon emission.

For polarised processes, these three regions can be considered when investigating spin asymmetries. In region 1, leading-twist collinear contributions to spin asymmetries are negligible. In region 2, where the TMD formalism applies, nonvanishing spin asymmetries are expected. As in region 3 the TMD approach can not be applied, the Sivers function is not defined there. This region is usually described in collinear QCD by means of the

"twist-3 formalism". The same formalism in principle can be extended to region 2, but it is important to stress that in this region the "twist-3" approach is equivalent to the TMDs one (see Refs. [28, 29]). The Sivers effect, described in TMDs approach via Sivers function, is described in region 2 in twist-3 approach by the $T_{F(x,x)}$ correlator which was shown to be directly related to the Sivers function.
Altogether, the increasing physics interest of the scientific community in the Sivers function in combination with the (given) Drell–Yan kinematics at COMPASS have hence led to the proposal to study TMD-induced spin effects in the region $\Lambda_{QCD} < p_T < Q$, *i.e.* for transverse dilepton momenta of about 1 GeV.

**Q 11:** *p57. What are the main systematics in the Sivers sign measurement.*

A: Accessing the Sivers function through the Drell–Yan process, we expect the same sources of systematic uncertainties as in the case of SIDIS measurements with a transversely polarised target performed at COMPASS so far (see *Sect. 3.6.4, p. 69* for more details). 'New' sources of systematic uncertainties in the DY measurement will be

- cell-to-cell 'migration' of events in the 3-cell polarised target which is due to the lower resolution along the $z$ axis caused by the hadron absorber;
- a different level of background, as in DY there exist background processes different from those in SIDIS.

In SIDIS, the main contributions to the overall systematic uncertainty arise from:

- acceptance variations from one target cell to another;
- stability of the apparatus.

According to the COMPASS experience with SIDIS measurements, the main contribution to the systematic uncertainty arises from the (in)stability of the apparatus, which can be controlled on a level of below 1%. Taking into account the simple topology of the Drell–Yan process (only two muons in the final state), there is no particular reason to expect a larger systematic uncertainty from these sources.
A detailed MC study as well as an analysis of real data were performed to study the possible new sources of systematic uncertainties mentioned above (for details see *Sect. 3.6.2* and *3.6.3, pp. 65–69*). In brief, the results are:

- The migration of events from one target cell to another will effectively dilute the asymmetries. From the 2009 beam test, which used a simplified absorber made of concrete and stainless steel, the migration was found to be below 3.5%. Besides the dilution, this migration causes each sample to effectively loose this percentage of polarisation, so that the average polarisation of each sample is reduced by 7%. An asymmetry of about 0.1, as it can be expected in DY based on fits to SIDIS data, would thus be reduced by about 0.007.
- The combinatorial background and the intrinsic charm contributions are negligible in the region of the dimuon invariant mass between 4 GeV/$c^2$ < $M_{\mu\mu}$ < 9 GeV/$c^2$. The results obtained from the 2009 beam test (*Sect. 3.6.2, p. 65*) and MC simulations show that both are certainly not dominant in the intermediate dilepton-mass range 2 GeV/$c^2$ < $M_{\mu\mu}$ < 2.5 GeV/$c^2$.

Taking into account that the final absorber will be entirely constructed from alumina ($Al_2O_3$) we will reduce the amount of multiple scattering by a factor of about 2.2 and, as a consequence, the cell-to-cell migration of events by the same factor. We therefore expect

Table 2: Veto-Inner (VI) trigger dead time as a function of the VI rate.

| VI trigger rate triggers per spill | VI dead time % |
|---|---|
| $1 \times 10^6$ | 1.8 |
| $5 \times 10^6$ | 4 |
| $10 \times 10^6$ | 8 |
| $23 \times 10^6$ | 18 |

that also in Drell–Yan measurements the main contribution to the systematic uncertainty will come from the stability of the apparatus.

**Q 12:** *For the DY results, is the 25% deadtime on the veto taken into account? Could the change of sign be seen with one year of data-taking. It looks so from the plot.*

A: In the 2009 DY beam test the Veto-Inner (VI) trigger rate was measured under the following conditions (November 22nd, run number 82338):

- 190 GeV $\pi^-$ beam;
- beam intensity $\approx 1.5 \times 10^8$ pions per spill;
- spill duration of 9.6 seconds.

The VI rate was found to be equal to $2.8 \times 10^6$ triggers per spill. In order to obtain the VI rate for future real DY data taking one has to scale this trigger rate up, corresponding to a pion beam intensity of $6.0 \times 10^8$ particles per spill, as it is envisaged for the planned DY program. The expected VI rate is then $2.8 \times 10^6 \times 4 = 11.2 \times 10^6$.
The dependence of the VI dead time as a function of the VI rate was measured in 2010 by the COMPASS trigger group, the results are presented in Table 2.
From this table, the VI dead time expected for the DY program is about 9%, for the current design of the VI trigger system. In the Proposal this number was taken into account together with the COMPASS DAQ system availability in the spectrometer availability of 85%.

Could the change of sign be seen in 1 year of DY data taking? We have to claim (or disclaim) an effect at the three-sigma level at least. In order to be able to give a quantitative estimate, we take the present knowledge on the conjectured SIDIS–DY universality of TMDs for granted. Then, using the fit of the available SIDIS data (see Ref. [30]), we expect about a 10% effect, so that, taking into account an expected statistical error of $\sigma \approx 2.3\%$, one year of data taking appears sufficient as can be seen from Fig. 20. For this estimate, a simple expressions for the Sivers asymmetry extraction at LO was used (more details can be found in Ref. [31]):

$$A_T^{\sin\phi_S}(x_a, x_b) \;=\; \frac{2}{f\,|\boldsymbol{S}_T|}\,\frac{\int \mathrm{d}\phi_S \mathrm{d}\phi\,\frac{\mathrm{d}N(x_a,x_b,\phi,\phi_S)}{\mathrm{d}\phi\,\mathrm{d}\phi_S}\sin\phi_S}{N(x_a,x_b)}\,.$$

The statistical accuracy, assuming a flat acceptance of the apparatus in the azimuthal angles $\phi_S$ and $\phi$ and in the polar angle $\theta$, is given by:

$$\delta\, A_T^{\sin\phi_S}(x_a, x_b) \;=\; \frac{1}{f\,|\boldsymbol{S}_T|}\,\frac{\sqrt{2}}{\sqrt{N(x_a,x_b)}}\,.$$

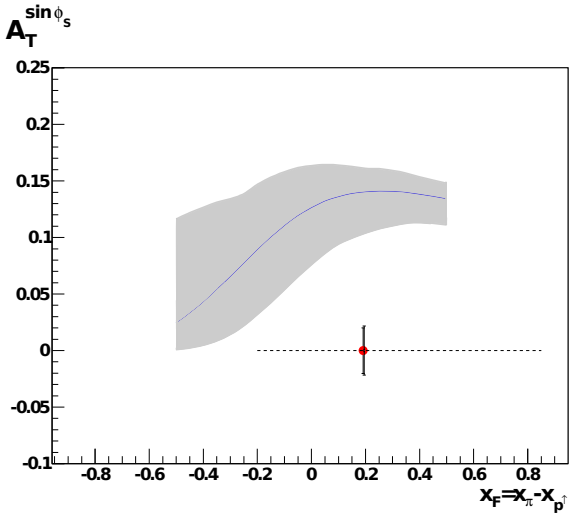


Figure 20: Expected statistical error of the Sivers asymmetry in the dimuon mass range 4 GeV/$c^2 \leq M_{\mu\mu} \leq$ 9 GeV/$c^2$, assuming one year of data taking (140 days). The smaller error bar denotes the statistical error, while the larger corresponds to the quadratic sum of statistical and systematic error. The theoretical prediction of the asymmetry from Anselmino *et al.* is also shown.

In our calculations of the projected statistical errors of asymmetries we used $|\boldsymbol{S}_T| = 90\%$ for the polarisation of the target material and $f = 0.22$ for the dilution factor. The total number of Drell–Yan events $N(x_a, x_b)$ was obtained by multiplying the DY event rate per day (*Table 8, 190 GeV pion beam, Sect. 3.5.1, p. 58*) and a total duration of a typical COMPASS run of 140 days per year.
However, given the total lack of experimental information on TMDs from Drell–Yan measurements and the strong requests of the community for proving the conjectured DY–SIDIS universality in detail, we consider it extremely worthwhile to envisage measurements not only of the sign but also of the amplitude and the shape of the Sivers function. For that purpose one year of data taking is clearly not enough and (at least) two years of data taking should be envisaged. This is shown in Fig. 21 where we divide the expected statistics in three (left) and five bins (right), assuming two years of data taking (280 days).

**Q 13:** *There is apparently a question at which x to quote the Sivers, for instance in Figure 31. How did you choose the middle point.*

A: We plan to present the results of the Drell–Yan measurements over the range $-0.2 < x_F < 0.85$. This will avoid to deal with too large acceptance corrections. The $x_F$ values, at which the projected data points are shown, are the respective weighted mean of the $x_F$ distribution in the given bin as obtained from the best present knowledge encoded in the COMPASS Monte Carlo program. When projections are shown over several bins in $x_F$ (3 or 5 bins), the borders of these bins were chosen by dividing the above quoted $x_F$ range in a such way that the reconstructed $x_F$ distribution, *i.e.* the one corresponding to the experimentally measured one, contains approximately the same statistics in each bin.

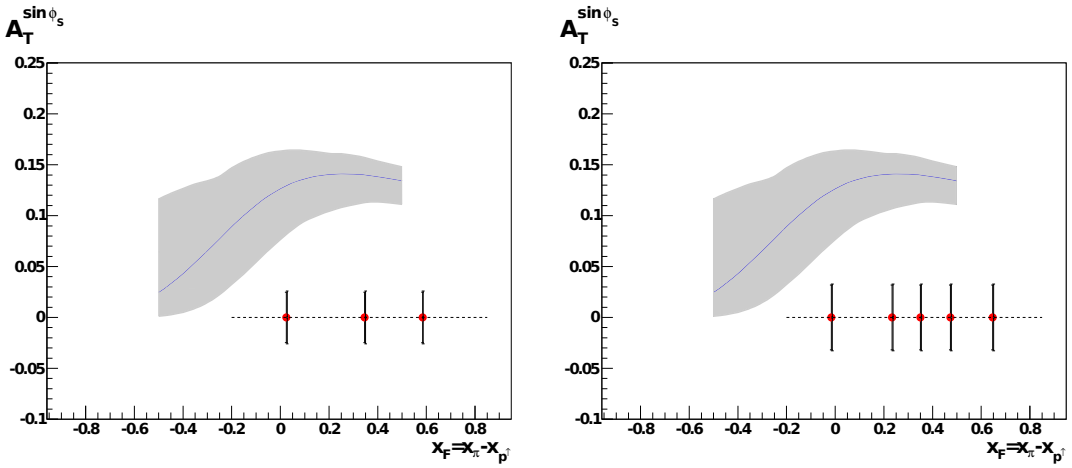


Figure 21: Expected statistical error of the Sivers asymmetry for a measurement in three (left) and five (right) bins in $x_F$ assuming two years of data taking (280 days). The smaller error bar is the statistical only, while the larger one corresponds to the quadratic sum of statistical and systematic errors. The theoretical prediction of the asymmetry from Anselmino *et al.* is also shown.

**Q 14:** *p51: how confident are we that J/psi can be used? Personal experience shows that there are too many uncontrolled theoretical uncertainties with J/Psi.*

A: The main goal of the COMPASS Drell–Yan program is to collect a sufficient amount of data in the so-called safe dimuon invariant mass region 4–9 GeV, where the theoretical formalism using TMDs is very well elaborated and the interpretation of the data is straight forward. Given the COMPASS kinematics and the design of this measurement, the $J/\psi$ data will come as a by-product. As the $J/\psi$ production cross-section is a factor of $\approx 30$ higher than the DY cross-section in the dimuon invariant mass range 4–9 GeV, it looks reasonable to use the $J/\psi$ data to study nucleon spin effects in this region as well as the formation mechanism of the $J/\psi$.
For the moment, existing theoretical models describe the $J/\psi$ production mechanism in the unpolarised process $H_aH_b \to J/\psi\ X \to l^+l^-X$. The most widely used model is the "gluon evaporation" model (see *Sect. 3.3.5* and references therein). This model allows to quantitatively control the quark and gluon contributions and to estimate when the former becomes dominant. In the COMPASS kinematic range and in the absence of a general theoretical model that can quantitatively describe the $J/\psi$ production mechanism, a model based on the close analogy (duality) between the Drell–Yan process $H_aH_b \to \gamma^*X \to l^+l^-X$ and $J/\psi$ production $H_aH_b \to J/\psi X \to l^+l^-X$ can be explored (see *Sect. 3.3.5*).
Assuming that the gluon-evaporation model can also be applied to a singly polarised DY process, we can expect that at COMPASS kinematics, *i.e.* for a fixed-target DY experiment with a 190 GeV pion beam, the contributions to the cross-section from the quark and gluon PDFs $q(x)$ and $g(x)$ are approximately the same. Hence the duality model applies only to a part of the data, which leads to a strong model dependence when studying nucleon spin effects on the basis of $J/\psi$ data.

**Q 15:** *p62: to which extent will you control the systematics in the low mass region (2–2.5 GeV) with a S/B ratio of 1?*

A: Again, as in the case of the $J/\psi$ region, the data to be collected in the intermediate dimuon mass region (2 GeV/$c$–2.5 GeV/$c$) will be considered as a by-product, as the major physics results are planned to be extracted from the high-mass region. In the intermediate-mass region the combinatorial $\mu^+\mu^-$ background originating from pion and kaon decays is the most relevant source of background. Its size relative to that of the signal will depend on the beam intensity as it increases with the square of the intensity while the size of the signal increases linearly. Estimates based on the beam test performed in 2009 indicate a S/B ratio of about 0.4 to be expected under the running conditions of future DY data taking.

The amount and a possible ('fake') spin asymmetry of same-sign muon pairs can be used to correct the measured DY spin asymmetry. The systematic uncertainty of the latter due to combinatorial background will hence be proportional to the statistical error of this fake spin-asymmetry. The size of the same-sign background sample will be about 0.7 of that of the opposite-sign sample, which contains both the signal and the background. Thus we expect that the systematic uncertainty of the measured spin asymmetry arising from combinatorial background will be less than a factor of 1.5 of the statistical error of the final spin-asymmetry measurement, *i.e.* in the case of the Sivers asymmetry it will stay below 1%.

On the other hand, in this mass range there exists also a background from pairs of correlated, opposite-sign muons that originate from the semi-leptonic decays of a $D$ and a $\bar{D}$ meson produced in the same interaction. The ratio of this contribution to that of DY pairs in the intermediate mass region amounts to about 14%. This estimate was obtained with Monte Carlo simulations using PYTHIA and using the measured cross-sections of $c\bar{c}$ and Drell–Yan production in pion-induced collisions (see *Sect. 3.6.3*). Here, for both contributions an $A$ dependence was assumed. The COMPASS spectrometer acceptance appears to be more favourable to the detection of DY pairs than to that of correlated $D\bar{D}$ pairs by a factor of about three. Nothing is known about the size of spin-asymmetries for $D\bar{D}$ production in singly-transversely-polarised pion–nucleon DY scattering. Hence any estimate has to be based on assumptions. We assume here that

- the $D\bar{D}$-induced asymmetry has a sign opposite to that of TMD-induced spin effects;
- the size of spin effects generated by the $D\bar{D}$ process is comparable to that of TMD-induced spin effects.

In such a situation, the expected background contribution to the measured spin asymmetry will not exceed 15% of the TMD-induced effect. Then, in the case of the Sivers asymmetry, where the expected value is about 0.05, this contribution would stay below 0.008.

# Detector

**Q 16:** *p86: which veto dead time do you expect to achieve with a higher granularity?*

A: There are several possibilities to reduce the dead time. The first one is to build a more sophisticated veto system, which vetoes not just every incoming muon not passing through the target, but only those which would really cause a trigger signal. First simulations show that the dead time could be reduced by a factor of two for the trigger system most affected by the beam halo. This solution would require two new hodoscopes upstream of the target with about 20 channels each and a size of $10 \times 10$ cm$^2$.
A second possibility is to relax the veto condition on the expense of a higher trigger rate. Online filtering could then be used to reduce the rate again. Note that inclusive triggers (*i.e.* only demanding a muon) have rates of about $1\text{–}2 \times 10^5$ for a beam intensity of $4 \times 10^7$ muons per second if no veto condition is applied. So the possibility to remove the veto completely and to use only filtering is excluded since a first level trigger rate of the order of $10^6$ per 9.6 s spill is too high.

**Q 17:** *Could you give us more details about the DVCS trigger and its tests with the data taken.*

A: The COMPASS trigger system as described in the Proposal has the ability to trigger on scattered muons in inclusive deep inelastic scattering events with an efficiency of about 80% in the $Q_2$ and $x_{bj}$ range of interest for the measurement of DVCS. Due to the high muon halo of about 30% of the incoming beam intensity a large fraction of the actual triggers is induced by halo muons despite the efficient veto system in front of the target. In the 2009 DVCS test run the trigger system was tested with the 40 cm long liquid hydrogen target. The comparison of filled and empty-target data has shown that in this case less than 10% of the observed trigger rate is due to hydrogen itself. Also the total rate is much higher than the expected DIS event rate of about 75 Hz at 100 GeV beam energy. At 160 GeV the DIS rate will be even lower.
This year we run for the first time with the fully inclusive trigger system with the polarised solid-state $NH_3$ target of 120 cm length including the newly built, large $Q^2$ trigger. The COMPASS DAQ is running very stably with a total accepted trigger rate of 25 kHz. Thus no specific DVCS trigger is required and data can be taken simultaneously for DVCS, DVMP and SIDIS measurements without prescaling of any of the trigger subsystems.
In addition the GANDALF system developed for the RPD readout has the possibility to produce a logic signal for each coincidence between the inner and the outer ring, which can be used for filtering or a high-level triggering mainly to allow very fast feedback during data taking.

**Q 18:** *p98: what is the path to decide on the various options for the ECAL upgrade? In general, the proposal for ECAL0 should be made more concrete. What is the required performance for this calorimeter? The location should be defined and the design suited for that location should be described. Also, why do you need the high MAPD granularity to read the fibers bundles?*

A: The COMPASS spectrometer is equipped with two electromagnetic calorimeters ECAL1 and ECAL2 used for neutral channels detection in both physics programmes with hadron

beam and muon beam. They are essential detectors for the COMPASS-II DVCS measurements. The requirements are common to all programmes:

- a good hermeticity and a large dynamical range,
- very good linearity and resolution in energy,
- a good time resolution,
- a precise calibration and on-line monitoring.

A specific requirement for the running with hadron beam is the radiation hardness, which has led to equip the central part of ECAL2 with radiation-hard Shashlik and GAMS modules. A significant upgrade of the readout electronics was realised for the 2008 and 2009 hadron runs.

Concerning data analysis, a task force is presently active with the goal to improve analysis and simulation tools and to obtain a precise calibration using the LED (Laser) monitoring signals of ECAL2 (ECAL1) and the $\pi^0$ signal (see answer to Question 2).

The calorimeter setup currently used for the muon running suffers from a non-uniformity in acceptance for photon detection, a consequence of some features indicated in Fig. 22. A project to upgrade the two ECALs is described in *Sect. 7.1*. In view of the magnitude of such project it is important to review in detail what needs to be taken into consideration in order to optimise the present ECALs setup.

ECAL1-ECAL2 horizontal gap: The transition in the horizontal direction between the inner edge of ECAL1 hole and the outer edge of the active surface of ECAL2 has a gap corresponding to about 1 mrad (see Fig. 22 top view). Four solutions are envisaged (in order of decreasing complexity and cost):

Option 1 - increase the horizontal size of ECAL2 by about 0.5 m at each side,

Option 2 - reduce the distance between the ECAL1 and ECAL2 calorimeters for which two options exist: a) move the ECAL2 calorimeter upstream of its nominal position by 6 to 7 m, b) move the ECAL1 calorimeter downstream of about 3 m.

Option 3 - reduce the horizontal size of the ECAL1 hole on each side by 10 to 12 cm,

SM2 vertical aperture: The vertical angular acceptance given by the SM2 aperture is slightly smaller than that of ECAL1 (see Fig. 22 side view). This limit is only seen when ECAL1 is at its upstream position which is the case for the muon setup.

HCAL1 hole: The vertical size of the HCAL1 hole is too small (see Fig. 22 side view), so that HCAL1 "stops" photons that would otherwise be detected in ECAL2. The size of the hole should be increased by 5 to 10 cm on both top and bottom. This modification is needed independently of the actual ECALs' positions.

For the 2008 and 2009 hadron running, the Option 2b was adopted to solve the horizontal acceptance gap: ECAL1 and the mechanically coupled HCAL1 hadronic calorimeter, first muon filter $\mu$F1 and second dipole magnet SM2 were all shifted downstream by 3 m. A drawback for the future COMPASS-II muon programme is the reduced ECAL1 acceptance, which in turn necessitates a smaller size of the inner hole of the large angle calorimeter ECAL0. This will reduce the overall acceptance for low-momentum and large-angle, charged particles and may lead to reduced performance for Deeply Virtual Meson Production (DVMP) physics.

Option 2a of moving ECAL2 upstream by 6 to 7 m is also envisaged. It implies a reshuffling of the charged-particle tracking between SM2 and ECAL2 and most likely modifications of the ECAL2/HCAL2 system and the 2nd hadron absorber (not shown in Fig. 22) which could have negative impact on the muon trigger performances.

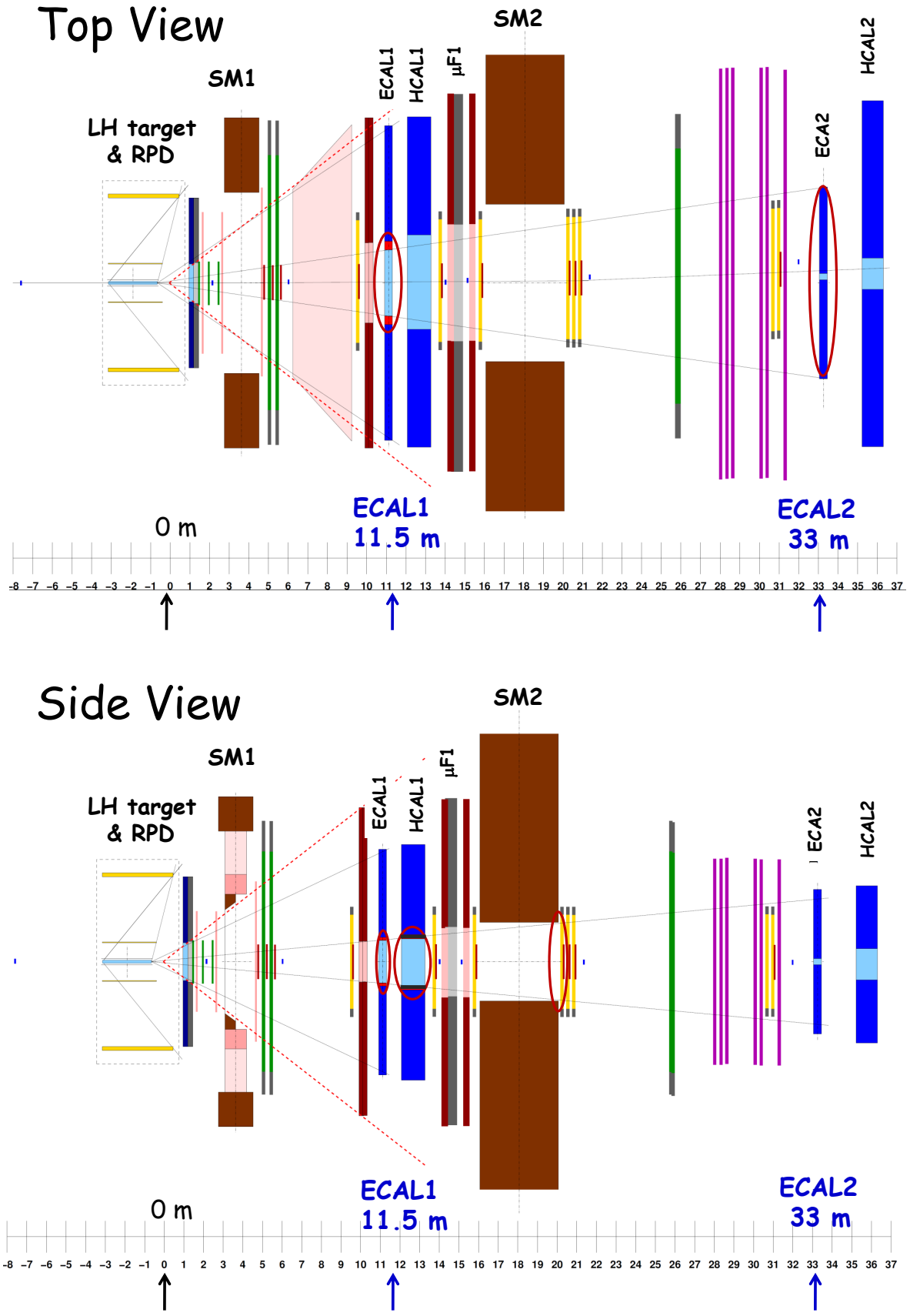


Figure 22: Present ECAL1 and ECAL2 layout for the muon programme, top (up) and side (down) views. Indicated within red circles are the critical parts of the setup.

The more rigorous solution to the horizontal acceptance gap is to fill it by extending the active surface of either ECAL2 (Option 1) or ECAL1 (Option 3). Option 1 provides higher granularity with the longest lever arm, *i.e.* the best angular resolution, however the photons need to traverse more material than if detected in ECAL1. Option 3 involves a relatively simple modification of the ECAL1 mechanical structure (also needed to adjust vertical size of central hole to the SM2 aperture) and a small amount of additional channels. Angular resolution for the detected photon is lower than in Option 1 but we expect a higher detection efficiency due to less material in $\gamma$'s path which can be beneficial for rejection of $\pi^0$ background.
Monte Carlo simulations are needed to provide more quantitative estimates. Important for GPD studies is the efficiency of the exclusivity cuts applied to select DVCS candidates. As shown in the answer to Question 3, these cuts contribute significantly to the rejection of background from exclusive $\pi^0$ production. We shall identify, which parameters are most sensitive for the quality of photon detection, and use them to weight the different upgrade options. We foresee the following steps:

- Reproduce with the MC the distributions of the variables used to apply exclusivity cuts for the DVCS 2009 test data. The MC should also reproduce accurately the azimuthal $\phi$ angle distribution dominated for medium and low $x_{Bj}$ values by the Bethe–Heitler process used as reference.
- Apply the MC simulation to the final setup with the 2.5 m long LH target for Option 1 - extension of ECAL2 and Option 3 - completion of ECAL1 hole. Note that a version of Option 3 referred in the proposal as "a new layout for ECAL1", which involves the replacement of the 572 Mainz cells of $7.5 \times 7.5$ cm$^2$ by 2296 GAMS cells of $3.8 \times 3.8$ cm$^2$ needs also to be evaluated.
- Compare the probability of photon absorption for the option of ECAL1 with reduced hole with the option of enlarged ECAL2.
- Compare the quality of the $2\gamma$ separation for $\pi^0$ detected in the central part of ECAL1 compared to that detected in the outer part of ECAL2.
- Finally, evaluate the impact of Option 2b with ECAL2 moved upstream on the tracking of charged particles and on the performances of the muon trigger and compare to the standard muon setup.

The time required to answer these questions is about three months with a dead line fixed at the end of 2010.

The electromagnetic calorimeter ECAL0 will supplement the COMPASS spectrometer for the GPD studies. The main tasks of the ECAL0 are the following:

- together with the ECAL1 and ECAL2, to ensure a hermeticity of the setup for photons from DVCS,
- to help in the reduction of $\pi^0$ background,
- to enlarge the kinematic domain of the DVCS events registered by COMPASS.

For these purposes the ECAL0 should detect photons in the energy range 0.2 GeV–30 GeV in the solid angle not covered by the ECAL1 and ECAL2.
The Technical Board of COMPASS, after various discussions, agreed that the optimal place for the calorimeter is just downstream of the RPD surrounding the liquid hydrogen target at $z = 0.85$ m (see *Figs. 57, p. 92*, and *65, p. 100*). At this position ECAL0 will have the dimensions and structure shown in Fig. 23. The calorimeter has a modular structure with 248 modules indicated by squares. The modules are mounted in a frame installed on a platform (not shown). A number of systems are necessary to operate the calorimeter.

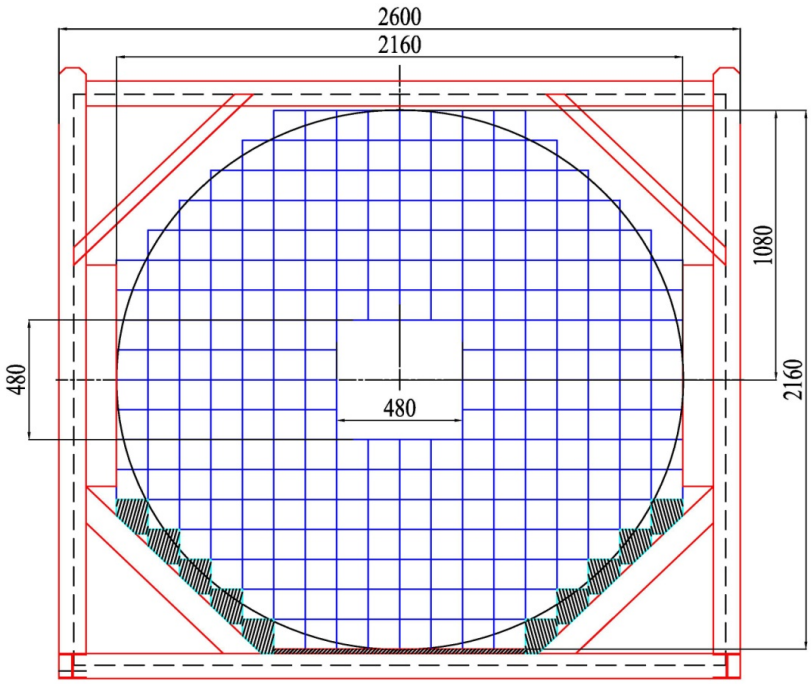


Figure 23: Dimension and structure of ECAL0.

These are the power supply system, the electronics, the read-out system, the temperature stabilisation system and the LED control system. The electronics and temperature stabilisation systems will be integrated into the modules. The read-out system will be based on the MSADCs used at COMPASS for other calorimeters. The LED control system will be similar to that of the HCAL1.
Based on a number of tests performed by the JINR Dubna group and described in the Proposal, the final structure of the module has been fixed. It is presented in Fig. 24 and the its main parameters are given in Table 3. The modules will be manufactured using the "shashlik" technology with scintillator layers molded under pressure. The scintillator layer will be subdivided in 9 cells, each of $4 \times 4$ cm$^2$. The light from each cell will be collected by fibres grouped in bundles glued to the Winston-cone light guides and attached to the

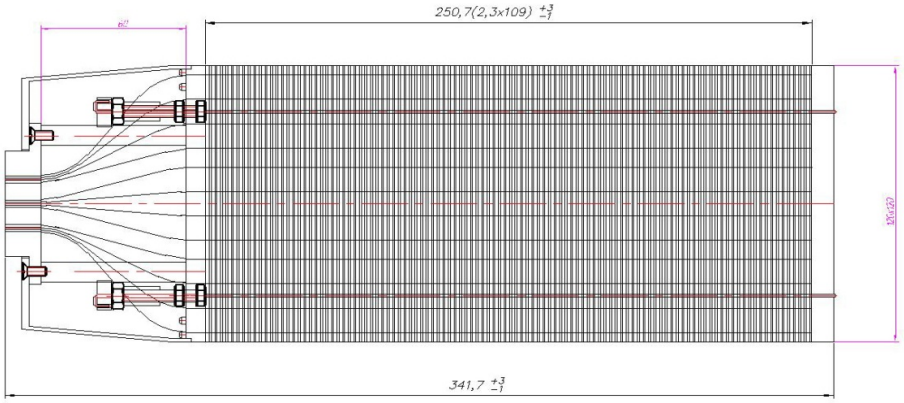


Figure 24: Structure of the ECAL0 module.

Table 3: Main characteristics of the ECAL0 module.

| | |
|---|---|
| Technology | Shashlik |
| Scintillator | Polystyrene, p-terphenyl POPOP, 109 layers |
| Absorber | Lead, 109 layers |
| Pb/Sc plates thickness, mm | 0.8/1.5 |
| Pb/Sc plates dimensions, cm | $12 \times 12$ (9 cells $4 \times 4$) |
| Molière radius, cm | 3.5 |
| Radiation length, cm | 1.64 |
| Number of towers | 9 |
| Number of fibres | 144 |
| Diam. of bundle, mm | 6.5 |

Table 4: Parameters of the MAPDs.

| Type | MAPD3A | MAPD3B | MAPD3N |
|---|---|---|---|
| Size, $mm^2$ | $3 \times 3$ | $3 \times 3$ | $3 \times 3$ |
| Pitch(pixel size), $\mu$m | 8(3) | 5(2) | 8(5) |
| Number of pixels | $\sim 135000$ | $\sim 360000$ | $\sim 135000$ |
| Bias voltage, V | $\sim 66.5$ | $\sim 70$ | $\sim 90$ |
| Gain, $\times 10^4$ | 2–3 | 1–1.5 | 5–7 |
| $\epsilon$, %($\lambda \approx 520$ nm) | 12 | 10 | 25 |

photodetector. A new technique of light collection and detection by MAPD photodiodes (Multipixel Avalanche PhotoDiode) is proposed. The MAPD is a novel photodetector with an intrinsic multipixel structure on a common silicon substrate. There are three types of the MAPDs produced by Zecotek. Their characteristics are shown in Table 4. The very high pixel density makes their response $A$ linear over a wide range of light intensities and thus of energies.
The number $N_f$ of firing MAPD pixels can be expressed as

$$A \approx N_f = N_t \left(1 - \exp\left(-\frac{\epsilon N_\gamma}{N_t}\right)\right),$$

where $N_t$ is a total number of pixels, $N_\gamma$ is the number of impinging photons and $\epsilon$ is the photon detection efficiency of the MAPD. When $N_\gamma \ll N_t$, the number of fired cells is proportional to $N_\gamma$. A finite number of pixels $N_t$ results in a deviation from linearity of the MAPD signals with increasing light intensity, *i.e.* $N_\gamma$. When about 50% of the cells fire at the same time (corresponding to about 35 GeV photon energy), the deviation from the linearity approaches 20%.
All three types of MAPDs satisfy the ECAL0 requirements formulated in the Proposal. The particular type of MAPD, to be used in ECAL0, will be chosen during the comparative studies at COMPASS in October 2010. The main goals of these tests will be behaviour of the MAPD characteristics vs. beam intensity in the presence of the muon beam halo.

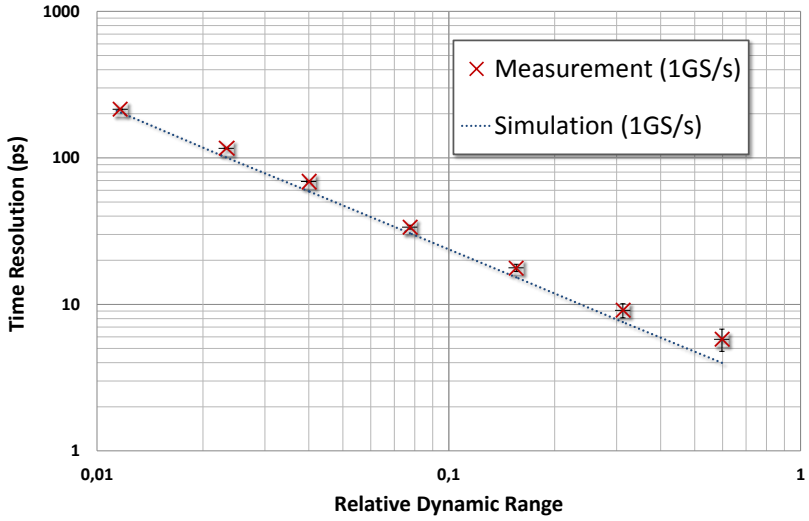


Figure 25: Measured time resolution of the GANDALF board at a sampling rate of $10^9$ samples per second as function of the pulse height. This quantity is compared to a full simulation of the GANDALF board.

The MAPD output parameters depend on temperature. It will be stabilised within 0.2 C by Peltier elements. The prototype of such a cooler has been successfully tested.

**Q 19:** *Section 6.2 How will the functionality of the RPD with the new GANDALF boards be tested. It needs to be demonstrated that the required timing resolution can be achieved.*

A: The timing resolution on the TOF (300 ps) is dominated by the resolution of the ring-A element for which the light output is low due to its small thickness of 4 mm. The requirement for the GANDALF system has been measured using test pulses and results are displayed in Fig. 25. It shows that the contribution of the board is 200 ps for a 50 mV signal and below 100 ps for signals 100 mV and higher. The contribution to the TOF resolution ($TOF = (t_B^{up} + t_B^{down})/2 - (t_A^{up} + t_A^{down})/2$) will always be smaller than 200 ps. A cosmics test-bench using the long RPD prototype scintillator counters (characteristics are listed in *Table 18*) with readout using the GANDALF system has been installed at Saclay and will provide a measurement of timing resolution for minimum-ionising particles, which represents the least favourable case in term of light output and hence signal amplitude. Other functionalities of the GANDALF board involving signal processing will also be evaluated with the cosmic test-bench.

# General

**Q 20:** *We would like to have an idea of the manpower, how will be this shared between the different analysis topics.*

A: A large fraction of the analysis procedures is in common for the various physics programmes, which all are all facets of the common interest in hadron physics and manifestations of QCD. This applies in the first place to the largely programme-independent reconstruction and Monte Carlo codes and the general physics analysis tools, but there are also synergies in dedicated methods, *e.g.* luminosity determinations. Like COMPASSalso COMPASS-II will be a joined effort where a particular group is often involved in several physics programmes. This opens a certain flexibility in analysis-manpower planning.
Triggered by the referees' question and although we did not yet plan in-depth for the analysis manpower, which anyway will have to be adapted to the actual situation in the future, insight in the manpower situation can be gained from the present situation.
Presently in COMPASS we have about 40 Ph.D. students and 60 postdocs/senior physicists involved in analysis. In addition about 20 diploma/master students contribute to the analysis effort. A clear attribution to a certain physics programme and the expected future development are ambiguous. Table 5 represents a best guess rather than a rigorous classification. It is however indicative the relative analysis strength in manpower of the various physics programmes in the future. For the Table the manpower presently involved in DY and transversity has been combined into one column (DY) as has been the ChPT and spectroscopy related manpower (ChPT). SIDIS here means the unpolarised SIDIS done in parallel with the DVCS/GPD studies as described in our proposal.
It should be noted that in particular the border between GPD and SIDIS is rather ambiguous and will certainly evolve with time. It must also be recalled that a large fraction of work listed in Table 5 is programme-independent and thus the distribution of manpower is in fact even more uniform than displayed in the Table. Taking into account the manpower mainly involved in hardware, this applies even more. Given the present situation and distribution of manpower over the various topics, the situation looks rather balanced and well adapted to the proposed measurements.

**Q 21:** *What is the level of present institutes commitments for their contributions to the upgrades?*

A: All Group Leaders from the Institutions listed in the author's part of the Proposal fully support the physics programme of COMPASS-II as well as the list of projects developed in *Table 20, pp. 117–118*. The tentative cost and responsibility sharing listed in *Table 20*, was initially discussed in the COMPASS Group Leader's Board on March 19, 2010, following a session of the Collaboration meeting dedicated to the Proposal. Issues arising were

Table 5: Best guess of future analysis manpower based on the presently people excluding diploma/master students.

| | GPD | SIDIS | DY | ChPT | total |
|---|---|---|---|---|---|
| Ph.D. students | 14 | 6 | 10 | 11 | 41 |
| Postdocs and seniors | 16 | 13 | 18 | 18 | 65 |

followed up in the next weeks before in a special session of the Group Leader's Board on May 5, the final version was approved by the Group Leaders. Obviously, the discussion on principal responsibilities had started much earlier.
The discussion of cost sharing with the funding agencies has started. However, it is obvious that at the present status no firm commitments can be expected. This can only happen after the proposal has been recommended by the SPSC for approval to the RB.
The involvement of JINR in the collaborative effort of the ECAL0 construction has been discussed with JINR from whom the main contribution is expected. This contribution has been confirmed to the COMPASS co-spokesperson G. Mallot during his visit to Dubna on June 21–22, 2010. The JINR LHEP director V. Kekelidze and the JINR vice director R. Lednicky supported the COMPASS-II physics programme and the JINR responsibilities for the existing MW1 and HCAL1 detectors as well as for participation in the construction of the ECAL0 as outlined in the COMPASS-II Proposal.
The RPD project has been discussed and defended in several meetings at CEA/Saclay and tentatively been included into the internal planing. The specifications will be finalised just after the September SPSC meeting and provided as input to a CEA-IRFU project review scheduled for November 19, 2010. The responsibilities for existing CEA/Saclay equipment will be continued. Other responsibilities of CEA/Saclay listed in *Table 20* are under discussion. Substantial support was signalled by CEA-IRFU in case the COMPASS-II proposal is recommended by the SPSC.
The COMPASS-II project has been presented regularly at INFN Committee meetings. The last presentation took place on May 19, after the submission of our Proposal. Up to now, no negative comments have been put forward and no show-stoppers are at the horizon. The discussions will be resumed in September 2010.

**Q 22:** *We would like to see more details about the new groups.*

A: Interest in joining COMPASS-II has been signalled by the following groups:

**Prof. Hartmut Schmieden**,
Physikalisches Institut, Universität Bonn, Germany:
Prof. Schmieden plans to join COMPASS already in 2010 to prepare for future activities in COMPASS-II. He is primarily interested in the transverse spin structure of the nucleon and GPDs. Initially, his group plans to involve a postdoc and two Ph.D. students in COMPASS. For COMPASS-II he will consider an enlargement of this involvement subject to funding by BMBF.

**Prof. Dr. Paul Reimer**,
Argonne National Laboratory, Argonne, IL, USA:
The Argonne MEP group is composed of six staff physicists along with three to six postdocs and two engineers. The group has extensive experience both in Drell–Yan (Fermilab E-866/NuSea and Fermilab E-906/SeaQuest) and in SIDIS (DESY HERMES) measurements as well as in hardware.
In case the group decides to join COMPASS-II, its involvement would be something equivalent to two FTE staff members and 75% of a postdoc. This level of commitment could not begin until after E-906/SeaQuest at Fermilab is running well and has its first year of data in hand – probably in 2012 or 13. Before then, we might be able to on the order of

50% of a staff person. A close collaboration with the group of Matthias Grosse Perdekamp is envisaged in case both groups join.

**Prof. Matthias Grosse Perdekamp**,
University of Illinois, Urbana-Champaign, IL, USA:
The Nuclear Physics Laboratory (NPL) at the University of Illinois consists presently of 5 faculty, 2 senior research scientists, 7 postdocs, 22 graduate students and three technicians. The group pursues a broad experimental program that includes measurements in deep inelastic scattering (HERMES at DESY) and proton–proton collisions (PHENIX at RHIC and SeaQuest at FNAL) that aim to explore the spin structure of the nucleon. NPL is funded through the National Science Foundation (NSF).
The PHENIX group at the UIUC NPL is interested to work on the COMPASS-II experiment at CERN and will seek funding to support its participation from the NSF. If successful, we anticipate joining COMPASS-II with 1 faculty, 1 postdoc and 2 graduate students. We expect that the postdoc and the 2 graduate students will be stationed at CERN. The group plans to join after the completion of the UIUC-led RPC based muon trigger upgrade in PHENIX.

**Q 23:** *As already mentioned, we would like to see a detailed schedule of the detector upgrades. It needs to show a scenario starting basically at the end of this year and covering the time until the last detector upgrade should be finished. It should show for each detector component to be upgraded the main phases of the project and it should contain milestones which allow to track the progress. Based on this schedule* COMPASS *should explain the sequence in which they want to take data, covering the full program. I think that we need to have an end date for this program (assuming that the accelerators deliver beams as expected). In addition it would be helpful to have as a table the hardware upgrades required for each type of measurement, indicating which part is absolutely needed and which is a nice to have.*

A: The planning for the various detector upgrades is being developed. The elements already defined and presented below demonstrate that the schedule given at the end of the Executive Summary (*p. 6*) is realistic (apart from the fact that now an accelerator shutdown is scheduled for 2012). The work on the planing continues and an update will be provided shortly before the September SPSC meeting. The total duration of the proposed measurements is clearly defined in the Executive Summary of the Proposal and will last five years assuming a beam delivery similar to the present situation.

RPD:
Important input to the performances and final design of the Recoil Proton Detector (RPD) for the GPD studies for COMPASS-II has been obtained from:

- tests on the COMPASS muon beam of the MuRex 4 m long prototype of 30° angular aperture performed on the M2 muon beam,
- the realisation of a 1 m long RPD for the COMPASS hadron running in 2008 and 2009, also used for the DVCS test runs. The results of these tests, summarised in *Table 18, p. 95*, have allowed us to freeze the main parameters of the two-layer scintillator system needed to achieve the final design as sketched in *Fig. 53*.

Figure 26 shows the foreseen planning which assumes a green light from SPSC and a starting date beginning of October. The specifications will be finalised just after the

September SPSC meeting and provided as input to a CEA-IRFU project review foreseen November 19 where the required human and technical resources from CEA will be agreed upon and frozen (mentioned as well in A21).

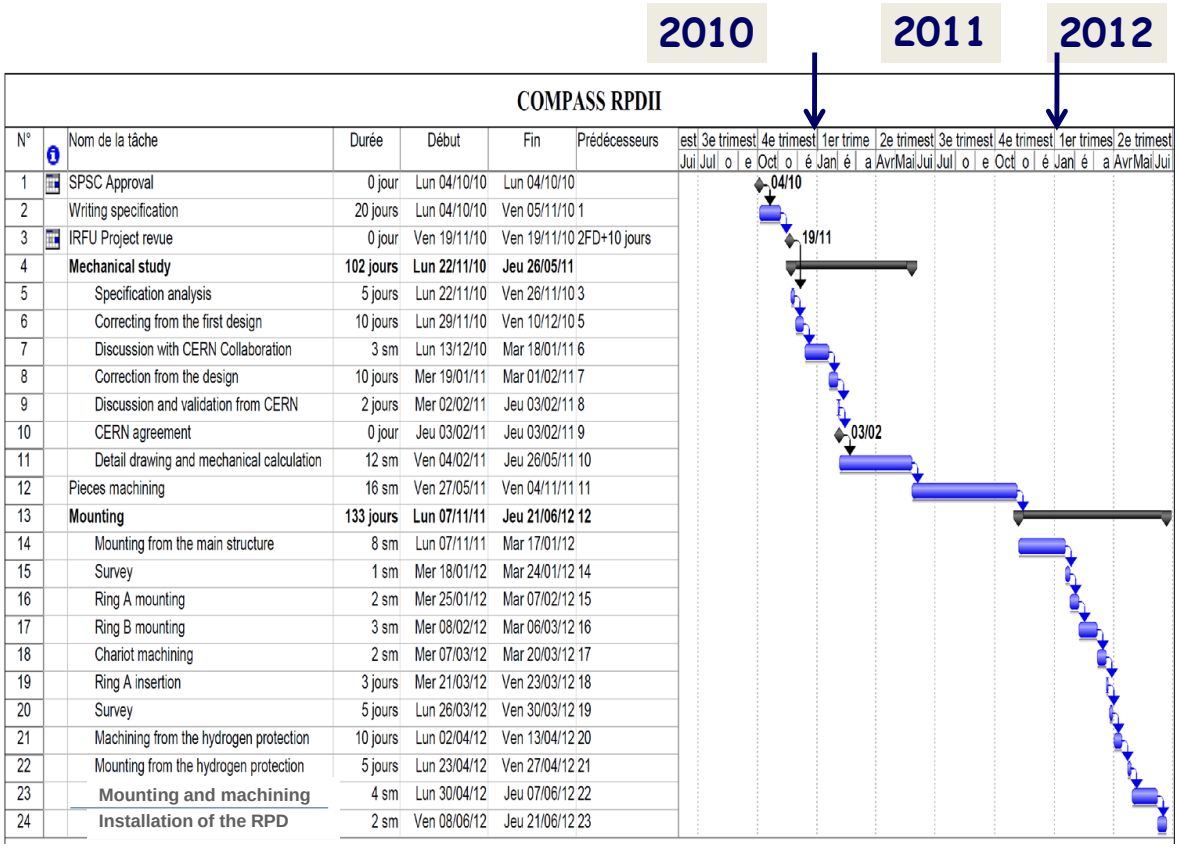


| N° | Nom de la tâche | Durée | Début | Fin | Prédécesseurs |
|---|---|---|---|---|---|
| 1 | SPSC Approval | 0 jour | Lun 04/10/10 | Lun 04/10/10 | |
| 2 | Writing specification | 20 jours | Lun 04/10/10 | Ven 05/11/10 | 1 |
| 3 | IRFU Project revue | 0 jour | Ven 19/11/10 | Ven 19/11/10 | 2FD+10 jours |
| 4 | **Mechanical study** | **102 jours** | **Lun 22/11/10** | **Jeu 26/05/11** | |
| 5 | Specification analysis | 5 jours | Lun 22/11/10 | Ven 26/11/10 | 3 |
| 6 | Correcting from the first design | 10 jours | Lun 29/11/10 | Ven 10/12/10 | 5 |
| 7 | Discussion with CERN Collaboration | 3 sm | Lun 13/12/10 | Mar 18/01/11 | 6 |
| 8 | Correction from the design | 10 jours | Mer 19/01/11 | Mar 01/02/11 | 7 |
| 9 | Discussion and validation from CERN | 2 jours | Mer 02/02/11 | Jeu 03/02/11 | 8 |
| 10 | CERN agreement | 0 jour | Jeu 03/02/11 | Jeu 03/02/11 | 9 |
| 11 | Detail drawing and mechanical calculation | 12 sm | Ven 04/02/11 | Jeu 26/05/11 | 10 |
| 12 | Pieces machining | 16 sm | Ven 27/05/11 | Ven 04/11/11 | 11 |
| 13 | **Mounting** | **133 jours** | **Lun 07/11/11** | **Jeu 21/06/12** | 12 |
| 14 | Mounting from the main structure | 8 sm | Lun 07/11/11 | Mar 17/01/12 | |
| 15 | Survey | 1 sm | Mer 18/01/12 | Mar 24/01/12 | 14 |
| 16 | Ring A mounting | 2 sm | Mer 25/01/12 | Mar 07/02/12 | 15 |
| 17 | Ring B mounting | 3 sm | Mer 08/02/12 | Mar 06/03/12 | 16 |
| 18 | Chariot machining | 2 sm | Mer 07/03/12 | Mar 20/03/12 | 17 |
| 19 | Ring A insertion | 3 jours | Mer 21/03/12 | Ven 23/03/12 | 18 |
| 20 | Survey | 5 jours | Lun 26/03/12 | Ven 30/03/12 | 19 |
| 21 | Machining from the hydrogen protection | 10 jours | Lun 02/04/12 | Ven 13/04/12 | 20 |
| 22 | Mounting from the hydrogen protection | 5 jours | Lun 23/04/12 | Ven 27/04/12 | 21 |
| 23 | Mounting and machining | 4 sm | Lun 30/04/12 | Jeu 07/06/12 | 22 |
| 24 | Installation of the RPD | 2 sm | Ven 08/06/12 | Jeu 21/06/12 | 23 |

Figure 26: Planning for construction, testing and installation of the Recoil Proton Detector for COMPASS-II

A test bench has been installed at Saclay and preparatory work has already started concerning the following items:

- an option of using MAPDs for the read out of the Ring A scintillators is under study, (keeping the standard photomultipliers as back up solution),
- testing of the GANDALF readout system on both Ring A and Ring B prototype detectors,
- comparison of two types of PMTs on Ring B, since the originally foreseen PMT may not be available,
- Optimisation of the light guides which should deviate the light from the scintillators of Ring B by 90°.

Answers to these questions should be given by the end of 2010. The ordering of the scintillator for Ring B and Ring A are presently programmed for October 2010 and January 2011 respectively. Note that before the final assembly, the scintillators and PMTs (MAPDs) will be tested on the test bench.

ECAL0:

| | | |
|---|---|---|
| 2010 | 1 | Comparative studies of the MAPD types with the existing ECAL0 module prototype . Three types of the MAPD will be tested at COMPASS: MAPD-3A, 3B and 3N. |
| | 2 | Construction of the ECAL0 $3 \times 3$ matrix as a preproduction series. |
| | 3 | Preparation of the equipment and technology for the mass production |
| 2011 | 1 | Tests of the $3 \times 3$ matrix at CERN. |
| | 2 | Presentation of the Internal JINR COMPASS-II Proposal at the JINR PAC meeting in January: JINR participation and requests for financing. |
| | 3 | Beginning of the ECAL0 construction. |
| | 4 | Production of MAPDs. |
| | 5 | Design and production of the frame and support. |
| 2012 | 1 | End of the ECAL0 module production |
| | 2 | Assembly of detector and installation in EHN2. |

Drell–Yan:

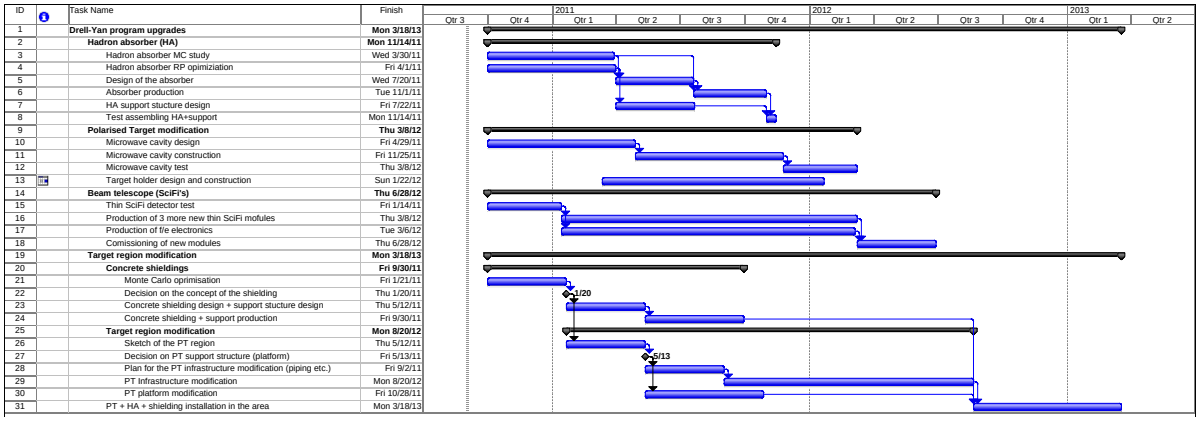


Figure 27: Planning for construction, testing and installation of upgrades for the DY programme.

RICH:

1. Completion of principle studies, including laboratory measurements and test beam exercises by October 2011.
   Corresponding milestone: complete principle project.
2. Completing detailed detector design by December 2011.
   Corresponding milestone: detector drawings available.
3. Constructions completed by March 2013.
   Corresponding milestone: detectors ready.
4. Installation possible in late Spring 2013.

Relevanz of upgrades for the various physics programmes:
In the following we give an indication for which programme the various upgrades are essential (++), beneficial (+) and not needed (−).

| Item | GPD | SIDIS | DY | ChPT |
|---|---|---|---|---|
| Scintillating fibres | + | + | ++ | + |
| Silicon | + | + | − | ++ |
| Pixel MM | + | + | + | + |
| ECAL0 | ++ | + | − | + |
| ECAL1 upgrade | ++ | + | − | + |
| ECAL2 monitoring | ++ | + | − | ++ |
| HCAL1 modification | ++ | − | − | − |
| RPD | ++ | − | − | − |
| LH-target | ++ | ++ | − | − |
| RICH upgrade | + | ++ | − | − |
| CEDAR upgrade | − | − | + | + |
| Polarised Target | − | − | ++ | − |
| Hadron Absorber | − | − | ++ | − |
| Veto | ++ | + | + | − |
| DAQ | ++ | ++ | ++ | ++ |
| DCS | + | + | + | + |

**References**


[1] Yu. M. Antipov *et al.*, Phys. Lett. **B121** (1983) 445.
[2] Yu. M. Antipov *et al.*, Z. Phys. **C26** (1985) 495.
[3] T. A. Aibergenov *et al.*, Czech. J. Phys. **B36** (1986) 948–951.
[4] J. Ahrens *et al.*, Eur. Phys. J. **A23** (2005) 113–127.
[5] Ch. Berger *et al.* [PLUTO], Z. Phys. **C26** (1984) 199.
[6] A. Courau *et al.*, Nucl. Phys. **B271** (1986) 1–20.
[7] Z. Ajaltouni *et al.*, in *VII Int. workshop on photon-photon collision*, Paris, France, 1986.
[8] D. Babusci *et al.*, Phys. Lett. **B277** (1992) 158–162.
[9] L. V. Fil'kov and V. L. Kashevarov, Phys. Rev. **C73** (2006) 035210.
[10] A. E. Kaloshin and V. V. Serebryakov, Z. Phys. **C64** (1994) 689–694.
[11] K. Nakamura *et al.* [Particle Data Group], J. Phys. G **37** (2010) 075021.
[12] M. Pennington, in L. Maiani *et al.*, eds., *The* $2^{\text{nd}}$ *DAΦNE Physics Handbook*, 1995, Frascati, Italy: INFN (1995) 1202 p.
[13] N. Kaiser and U. Meissner, July 2010, private communication.
[14] O. Kouznetsov and J. ter Wolbeek, *Presentations at an internal COMPASS meeting in Freiburg*, July 2010.
[15] J. Bernhard *et al.*, *The first observation of exclusive single-photon muoproduction at compass in 2008 dvcs test run*, April 2009, COMPASS Note 2009-4, `http://wwwcompass.cern.ch/compass/notes_public/2009-4.pdf`.
[16] J. Bernhard *et al.*, *A new analysis of the 2008 dvcs test run data using the precise timing information for photons detected in the electromagnetic calorimeters*

*ecal1/ecal2*, October 2009, COMPASS Note 2009-11, http://wwwcompass.cern.ch/compass/notes_public/2009-11.pdf.
[17] E. Burtin *et al.*, *A new analysis of the 2008 dvcs test run data using the precise timing information for photons detected in the electromagnetic calorimeters ecal1/ecal2.*, June 2010, COMPASS Note 2010-6, http://wwwcompass.cern.ch/compass/notes_public/2010-6.pdf.
[18] A. Ferrero, July 2010, private communication, August 17, 2010.
[19] M. Vanderhaeghen *et al.*, Phys. Rev. Lett. **80** (1998) 5064–5067.
[20] A. Aktas *et al.* [H1], Eur. Phys. J. **C46** (2006) 585–603.
[21] Ch. Höppner *et al.*, *Luminosity 2004 W38-W31*, September 2010, COMPASS Note 2010-10, http://wwwcompass.cern.ch/compass/notes_public/2010-10.pdf.
[22] J. Pretz, *Veto dead time & beam duty factor*, June 2010, COMPASS Note 2010-8, http://wwwcompass.cern.ch/compass/notes_public/2010-8.pdf.
[23] W. Käfer [COMPASS], [arXiv:0808.0114 [hep-ex]].
[24] F. Giordano and R. Lamb [HERMES], AIP Conf. Proc. **1149** (2009) 423–426.
[25] V. Barone *et al.*, Phys. Rev. **D81** (2010) 114026.
[26] M. Anselmino *et al.*, Nucl. Phys. Proc. Suppl. **191** (2009) 98–107.
[27] A. Bacchetta *et al.*, JHEP **08** (2008) 023.
[28] X. Ji *et al.*, Phys. Rev. **D73** (2006) 094017.
[29] X. Ji *et al.*, Phys. Rev. Lett. **97** (2006) 082002.
[30] M. Anselmino *et al.*, Phys. Rev. **D79** (2009) 054010.
[31] A. Kotzinian, February 2010, COMPASS Note 2010-2, http://wwwcompass.cern.ch/compass/notes_public/2010-2.pdf.